Dalton Transactions

RSC Publishing

PAPER

View Article Online
View Journal | View Issue

1,5-Diarylbiguanides and their nickel(II) complexes†

Cite this: *Dalton Trans.*, 2013, **42**, 2948

David A. McMorran,* C. John McAdam, Holly van der Salm and Keith C. Gordon

1,5-Diarylbiguanides, where the aryl groups are phenyl (**HL1**), 3,5-dimethylphenyl (**HL2**), 3,5-dimethoxyphenyl (**HL3**), 4-*t*-butylphenyl (**HL4**) or 4-bromophenyl (**HL5**), have been prepared and characterised. **HL3** and **HL5** have been structurally characterised by X-ray crystallography, which shows them to adopt the expected tautomeric form for biguanides. They have extensive hydrogen-bonding interactions in the solid state, involving the biguanide NH groups supported by, in the case of **HL3**, the OCH_3 aryl substituents or, in the case of **HL5**, Br···Br interactions. Reactions of **HL1–HL4** with $Ni(BF_4)_2$ gives complexes of the type $[Ni(\mathbf{HL})_2](BF_4)_2$, while reactions of **HL1–HL4** with $Ni(BF_4)_2$ and triethylamine give neutral complexes of the type $[Ni(\mathbf{L})_2]$, where the biguanide ligand has been deprotonated at the N_{ring} nitrogen. Both series of complexes were characterised in solution and the solid state. Cyclic voltammetry shows a largely irreversible Ni(II)/Ni(III) oxidation which becomes easier by *ca.* 70 mV upon ligand deprotonation, with more subtle variations resulting from the changes in aryl ring substituents. Infrared and ^{1}H NMR spectroscopies both provide evidence for ligand deprotonation leading to the chelate ring becoming increasingly aromatised. X-ray crystallographic analyses of five of the complexes also show changes in bond lengths and angles within the chelate ring, consistent with increased electron delocalisation. A variety of hydrogen bonding motifs involving the complex ions, counterions and solvent molecules are found. The results of DFT calculations on both cationic and neutral complexes provide calculated structures consistent with the experimental ones and these, along with the results of vibrational spectroscopic studies, provide further evidence for increased aromatisation upon deprotonation. The potential for the complexes to act as tectons for the rational assembly of hydrogen bonded metallosupramolecules is discussed and the X-ray structure of such an assembly, between $[Ni(\mathbf{L3})_2]$ and 1,8-naphthalimide, is presented.

Received 18th October 2012,
Accepted 7th December 2012

DOI: 10.1039/c2dt32483k

www.rsc.org/dalton

Introduction

The rational assembly of component molecules into larger supramolecular species continues to be a major theme in modern chemistry. In particular, the use of non-covalent interactions to drive the assembly of transition-metal containing components into new species with interesting structural and functional properties has received increasing attention.[1] Of the various non-covalent interactions available, the most attractive, in terms of strength and directionality, are hydrogen bonds. We,[2] and others,[3] have shown that, by incorporating suitable hydrogen bond donor and/or acceptor groups into the ligands, rational assembly of complex ions can be achieved, either directly with each other or to other molecular fragments with complementary hydrogen bonding groups. To advance this area of research, new ligands which incorporate hydrogen bonding motifs are required. Biguanide (**1**) was first reported in 1892[4] and, since then, various methods for the synthesis of **1** and its derivatives have been reported and several reviews have appeared.[5] While these molecules have received significant interest due to their varied biological properties,[6–10] the coordination chemistry of **1** itself has also been extensively studied, particular by Ray and co-workers.[11,12] These studies aimed to better understand the biological function of biguanide and also explore its ability to stabilise transition metals in high oxidations states (*e.g.* Ni(III)[13] and Ag(III)[14]). While a wide variety of transition metal ions are found to form stable complexes with **1**, it was only more recently, once X-ray structural data for **1** and its complexes were obtained, that the nature of the coordination itself was resolved. It is now known that, in the solid state, **1** adopts the tautomer shown in Scheme 1a,[5] in which an intramolecular hydrogen bond stabilises a largely planar conformation, whereas in complex ions, the neutral ligand coordinates as shown in Scheme 1b.

Metal complexes of **1** act as weak acids, with the hydrogen on the chelate ring nitrogen (N_{ring}) being readily lost[12]

Department of Chemistry, University of Otago, PO Box 56, Dunedin, New Zealand. E-mail: davidm@chemistry.otago.ac.nz; Fax: +64 03 479 7906; Tel: +64 03 479 7934

†Electronic supplementary information (ESI) available. CCDC 843769–843775. For ESI and crystallographic data in CIF or other electronic format see DOI: 10.1039/c2dt32483k

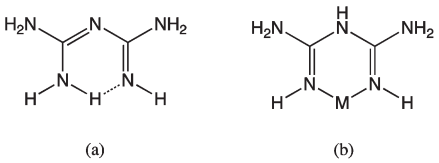

Scheme 1 Tautomeric forms of free (a) and coordinated (b) biguanide **1**.

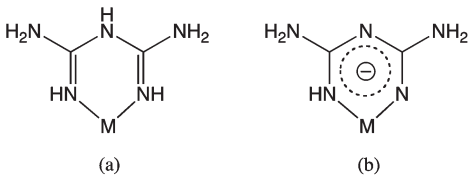

Scheme 2 Neutral (a) and deprotonated (b) forms of coordinated biguanide **1**.

(Scheme 2). The resulting delocalisation of charge within the chelate ring upon deprotonation has been demonstrated by a number of X-ray crystallographic studies, which show that the coordinated neutral ligand has C–N bond lengths in the order $C–N_{donor} < C–N_{terminal} < C–N_{ring}$ (with the $C–N_{donor}$ length often less than 1.3 Å), whereas coordinated deprotonated ligand has the order $C–N_{donor} < C–N_{ring} < C–N_{terminal}$, with the $C–N_{donor}$ lengthening and becoming more similar to the $C–N_{ring}$ length.[12] A characteristic decrease in the $C–N_{ring}–C$ bond angle from *ca.* 126° to *ca.* 120° is also observed.

Much literature exists on the coordination chemistry of **1**, and, to a lesser extent, derivatives of **1**, typically obtained by substitution at the donor or terminal nitrogen atoms.[13–15] Only one report of complexes involving 1,5-diaryl substituted biguanides exists, however, in which Masuda and coworkers describe the preparation of Ni(II) and Cu(II) complexes of deprotonated 1,5-diphenylbiguanide and demonstrate their potential as tectons for supramolecular species.[16] Given the obvious structural similarities of these complexes with melamine, a hydrogen bonding tecton *par excellence*,[17] it seems that a thorough exploration of the solution and solid-state chemistries of such compounds, so as to ascertain their potential for the construction of assemblies with interesting structural and functional properties, is warranted.

Consideration of the structures in Scheme 2 show that, in both cases, the biguanide ligand has great potential for acting as a tecton for assembly by hydrogen bonding.[18–20] Scheme 3 depicts the possible hydrogen bonding motifs that might be expected for the 1,5-diarylbiguanides in the current complexes. With the aryl rings in an *anti–anti* conformation (a) and (c), donor–donor–donor (DDD) and donor–acceptor–donor (DAD) triple hydrogen bonding motifs, respectively, are possible. In these cases, the $N_{donor}–H$ hydrogens may not be able to hydrogen bond due to the proximity of the aryl rings. Conversely, with the aryl rings in a *syn–syn* conformation, DDDD motifs, involving the $N_{donor}–H$ and $N_{aryl}–H$ hydrogens, are possible for complexes incorporating either the neutral and the deprotonated ligands. In this case, the N_{ring} position is potentially

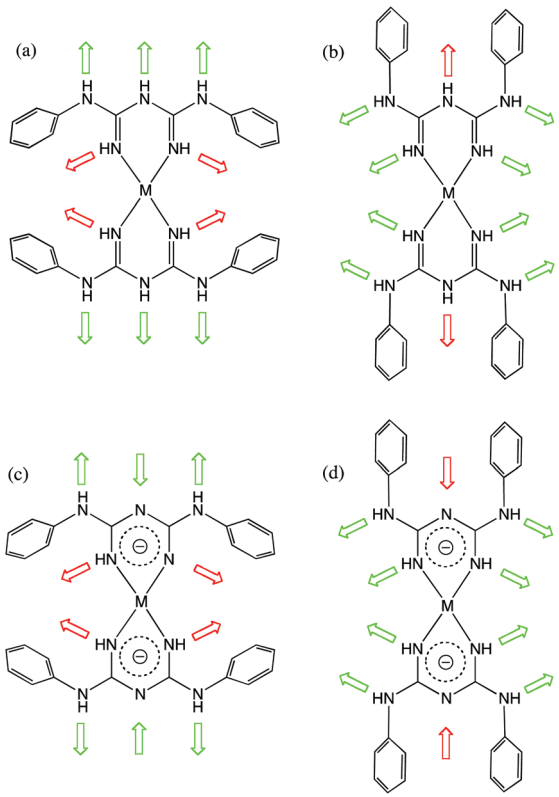

Scheme 3 Possible hydrogen bonding motifs (green arrows) for metal complexes of neutral {(a) and (b)} and deprotonated {(c) and (d)} diarylbiguanide ligands. Red arrows indicate hydrogen-bonding sites potentially blocked by adjacent aryl rings.

blocked by the two aryl rings. *Syn–anti* conformations might be expected to give intermediate situations.

In the current paper, a series of 1,5-diarylbiguanides and their nickel(II) complexes are reported. Based on previous studies,[16,21,22] it was expected that the use of Ni(II) would reliably give square planar species. Complexes, which contain either the ligands in their neutral form (giving complex salts) or in their deprotonated form (giving neutral complex species), have been synthesised and characterised, both in solution and in the solid state. DFT calculations are also used to characterise their electronic properties. As such, this is, to our knowledge, the first time that, within the one study, a thorough comparison of the chemistries of a series of complexes with both neutral and deprotonated biguanide ligands has been reported.

Results and discussion

The ligands **HL1–HL5** were prepared in a straightforward manner following the method described by Wuest and coworkers.[5a] Two equivalents of the hydrochloride salt of the respective anilines were refluxed with sodium dicyanamide overnight, with the free ligand being then obtained from the resulting hydrochloride salt by treatment with sodium

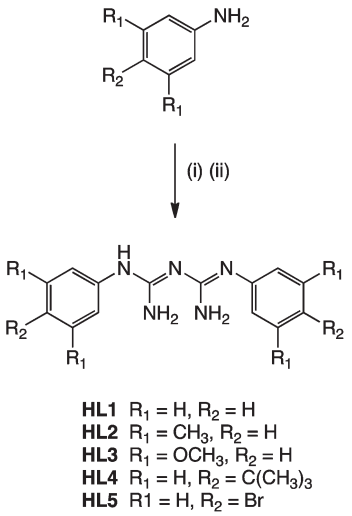

Scheme 4 Syntheses of 1,5-biarylbiguanides. (i) $NaN(CN)_2$, dil. HCl, reflux; (ii) $NaOCH_3$, methanol, RT.

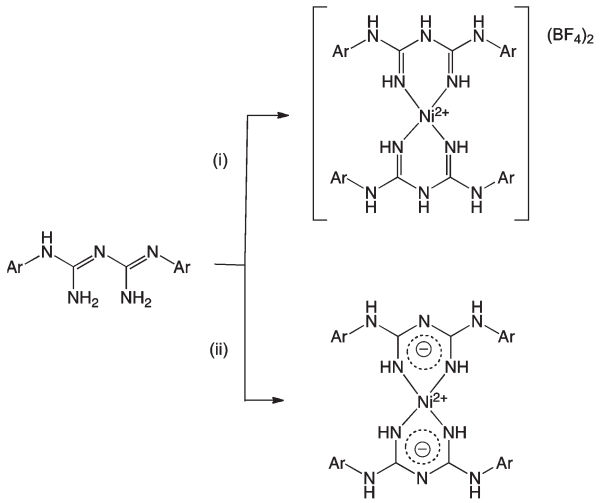

Scheme 5 Synthesis of nickel(II) complexes. (i) 1/2 equiv. $Ni(BF_4)_2{\cdot}6H_2O$, acetone, RT, (ii) 1/2 equiv. $Ni(BF_4)_2{\cdot}6H_2O$, 1 equiv. $(CH_3CH_2)_3N$, methanol, RT.

methoxide (Scheme 4). Ligands were obtained in good to high yield and in excellent purity directly from the reaction mixtures. The new ligands **HL3** and **HL4** were characterised by microanalysis, ESI-MS and IR and ^{1}H NMR spectroscopies. Reactions of **HL1** to **HL4** with 1/2 equiv. of $Ni(BF_4)_2{\cdot}6H_2O$ in acetone gave an orange-red solution which, upon addition of diethyl ether, gave the analytically pure $[Ni(\mathbf{HL})_2](BF_4)_2$ salts in good yield. Microanalyses and ESI-MS confirmed the desired 1 : 2 Ni : L ratio. Under the experimental conditions used for the ESI-MS, deprotonation of the ligands in the cationic nickel(II) complexes was observed.

Reactions between $Ni(BF_4)_2{\cdot}6H_2O$ and **HL5** under these conditions did not give precipitates in the same way. Orange solids could be isolated by addition of diethyl ether or petroleum ether to the orange reaction solutions, however microanalyses consistent with the desired complex could not be obtained. This may be due to nickel species formed in the solution reacting with the C–Br bonds in the ligands.[23] The natures of the products of these reactions were not explored further. It is further noted that attempts to prepare these complexes in methanol gave products for which correct microanalyses could not be obtained – the results suggested that partial ligand deprotonation occurs in this solvent, giving samples with non-stoichiometric numbers of counterions.

The reaction of each ligand with 1/2 equiv. of $Ni(BF_4)_2{\cdot}6H_2O$ in methanol, followed by addition of one equivalent of triethylamine, gave orange-red solutions which deposited orange precipitates. Microanalyses of these precipitates showed them to have a 1 : 2 Ni : L ratio and confirmed that the ligands had been successfully deprotonated as there were no counterions present. Again, reactions with **HL5** appeared to proceed differently and pure compounds could not be obtained. In the ESI-MS spectra, each pair of complexes ($[Ni(\mathbf{HL})_2](BF_4)_2$ and $[Ni(\mathbf{L})_2]$) gave essentially the same spectra, with the major peak corresponding to $[Ni(\mathbf{HL})(\mathbf{L})]^+$. Further, in some cases, peaks corresponding to DMF adducts were observed, suggesting that, in the DMF/CH_3CN solution used for the measurements, DMF molecules can readily hydrogen bond to the NH protons in the complex ions (Scheme 5).

While the infrared spectra of a number of simple biguanide complexes have been reported, there are few detailed comparative studies on pairs of complexes containing both the neutral and deprotonated ligands, respectively.[24,25] It might be expected that, upon deprotonation, the bond orders of the CN bonds in the chelate ring will become more similar, and this should result in the C=N stretches moving to lower energy and the C–N stretches moving to higher energy. Infrared spectra were recorded on both series of the present nickel complexes. In all cases, a series of weak peaks in the region *ca.* 3400–3050 cm^{-1} were observed, corresponding to N–H stretches. In the complexes containing neutral ligands, strong C=N bands and medium to strong C–N stretches were observed at *ca.* 1670–1600 cm^{-1} and 1050–990 cm^{-1}, respectively. This is consistent with spectra reported previously.[24] In contrast, spectra of the deprotonated ligands had no strong peaks in these areas (except for $[Ni(\mathbf{L3})_2]$ which had strong C–O bands at *ca.* 1150 cm^{-1}). Instead, strong peaks at *ca.* 1600–1450 cm^{-1} are observed. This is consistent with the proposal that, upon deprotonation, the chelate ring becomes increasing aromatised, thus lowering the bond order of the C=N bonds and increasing the bond order of the C–N bonds. A more detailed analysis of these effects is provided by DFT calculations and Raman spectra (*vide infra*).

^{1}H NMR spectra were recorded for the ligands and the complexes in various solvents. For comparison, spectra of all compounds were recorded in d_7-DMF, but the spectra of the ligands were also recorded in $CDCl_3$ and some of the complex spectra were also recorded in d_6-DMSO. It has been reported previously that signals corresponding to the NH protons in the ligands are poorly resolved[5a] and this was found to be the case in the current study. In d_7-DMF, extremely broad signals could be identified at *ca.* 6.4–7.2 ppm, while in d_6-DMSO and $CDCl_3$,

no peaks could be seen at all. This is presumably due to the NH protons being involved in hydrogen bonding interactions with solvent molecules. It has further been reported that the protonated salts of the ligands give much better resolved NH peaks in the ^{1}H NMR spectra.[5a] Similar results were found for the spectra of the nickel(II) complexes of the neutral ligand. A peak attributable to the N_{ring}–H proton is observed at *ca.* 9.6 ppm for each of the complexes. Two other peaks attributable to the other NH protons, are also observed; one of these remains at *ca.* 7.6 ppm for all the complexes, while the position of the second one varies from 7.27 ppm (for $[Ni(\mathbf{HL4})_2]^{2+}$) to 6.17 ppm (for $[Ni(\mathbf{HL3})_2]^{2+}$). The former peaks are therefore assigned to the N_{donor}–H hydrogens, while the latter are assigned to the N_{aryl}–H hydrogens, which would be expected to be more influenced by the natures of the substituents on the aryl rings. In each of the spectra, small peaks due to free ligands were also present, showing that, in DMF solvent, some degree of ligand dissociation occurs. In the case of $[Ni(\mathbf{HL2})_2]^{2+}$ a variable temperature study was carried out and this showed neither an increase in the amount of free ligand present, nor a coalescence of the peaks due to free and coordinated ligand.

In ^{1}H NMR spectra of the neutral nickel(II) complexes, the peak at *ca.* 9.6 ppm is lost, as expected. The peak at *ca.* 7.6 ppm, due to the coordinated N_{donor}–H hydrogens, sharpens and moves downfield to *ca.* 8 ppm (Fig. 1), consistent with the chelate ring becoming increasingly aromatic. However, peaks due to the N_{aryl}–H hydrogens could not be resolved (as was the case in the free ligands). The reason for this is not clear but it may be that these NH protons are involved in hydrogen bonding interactions with the DMF solvent molecules, consistent with the observations from the ESI-MS spectra. There was no evidence of free ligand in these solutions, suggesting that the deprotonated ligand is more strongly coordinated than the neutral ligand.

Previous studies on the UV/Visible spectra of cationic nickel(II) biguanide complexes report a single band at *ca.* 445 nm, consistent with a square planar geometry and, based on solvent studies, this was assigned to a metal centred $d_{xy} \rightarrow d_{x^2-y^2}$ ($^1A_{1g} \rightarrow {}^1A_{2g}$) transition.[25,26] UV/Visible spectra of the current complexes were recorded in DMF and, in each case, spectra consistent with a square planar d^8 system were found. For the cationic nickel(II) complexes, a single band at *ca.* 445 nm is observed (extinction coefficients 100–120 mol^{-1} L cm^{-1}), while for the neutral complexes, this band shifts to *ca.* 436 nm (extinction coefficients 110–170 mol^{-1} L cm^{-1}) and a low energy shoulder at *ca.* 490 nm is also observed. This small shift to higher energy implies that the deprotonated ligand is a better donor than the neutral ligand, as has previously been proposed for complexes of **1**.[25] Calculated spectra (*vide infra*) confirm this and show that the transitions are in fact metal–ligand charge transfer in nature.

The electrochemistry of the complexes was probed using cyclic voltammetry in DMF solution. Results are presented in Table 1 and representative voltammograms in Fig. 2 and S1.† Previous literature studies on similar biguanide systems have been performed in aqueous solution, making comparison with our results difficult.[27] For all complexes an anodic sweep at 100 mV s^{-1} gives rise to an irreversible feature attributed to the $Ni^{3+/2+}$ oxidation couple. The reversibility of this process improved with increasing scan rate (Fig. S1†). Sweeping to higher anodic potentials reveals another irreversible process *ca.* 1.2 V typical of amine oxidation.[28] Removal of the protons from $[Ni(\mathbf{HL})_2]^{2+}$ shifts E_{pa} for $[Ni(\mathbf{L})_2]$ approximately 70 mV cathodically, concordant with the increase in electron density at the nickel centre (Fig. 2).

Table 1 Electrochemistry data

	E_{pa}/V
$[Ni(\mathbf{HL1})_2](BF_4)_2$	0.79
$[Ni(\mathbf{HL2})_2](BF_4)_2$	0.77
$[Ni(\mathbf{HL3})_2](BF_4)_2$	0.80
$[Ni(\mathbf{HL4})_2](BF_4)_2$	0.76
$[Ni(\mathbf{L1})_2]$	0.72
$[Ni(\mathbf{L2})_2]$	0.69
$[Ni(\mathbf{L3})_2]$	0.75
$[Ni(\mathbf{L4})_2]$	0.69

Solutions ~1 × 10^{-3} mol L^{-1} in DMF with 0.1 M Bu_4NPF_6. Values referenced to $[Fc^*]^{+/0}$ = 0.00 V.

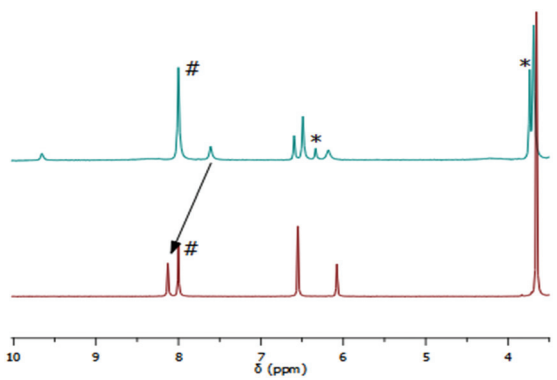

Fig. 1 ^{1}H NMR spectra of $[Ni(\mathbf{HL3})_2](BF_4)_2$ (top) and $[Ni(\mathbf{L3})_2]$ (bottom) in d_7-DMF solution. Arrow indicates movement of the N_{donor}–H hydrogen peak upon deprotonation. # solvent, * free ligand.

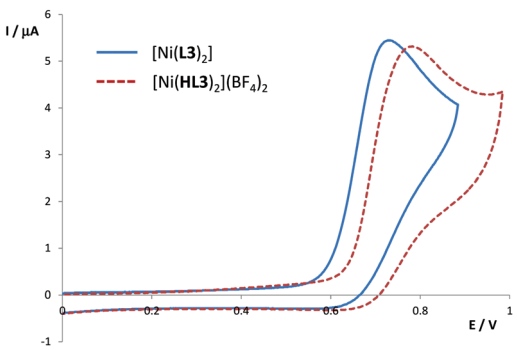

Fig. 2 Cyclic voltammograms of $[Ni(\mathbf{HL3})_2](BF_4)_2$ and $[Ni(\mathbf{L3})_2]$ (*ca.* 1 × 10^{-3} mol L^{-1} in DMF, 0.1 mol L^{-1} Bu_4NPF_6, 100 mV s^{-1}, referenced to $[Fc^*]^{+/0}$ = 0.00 V).

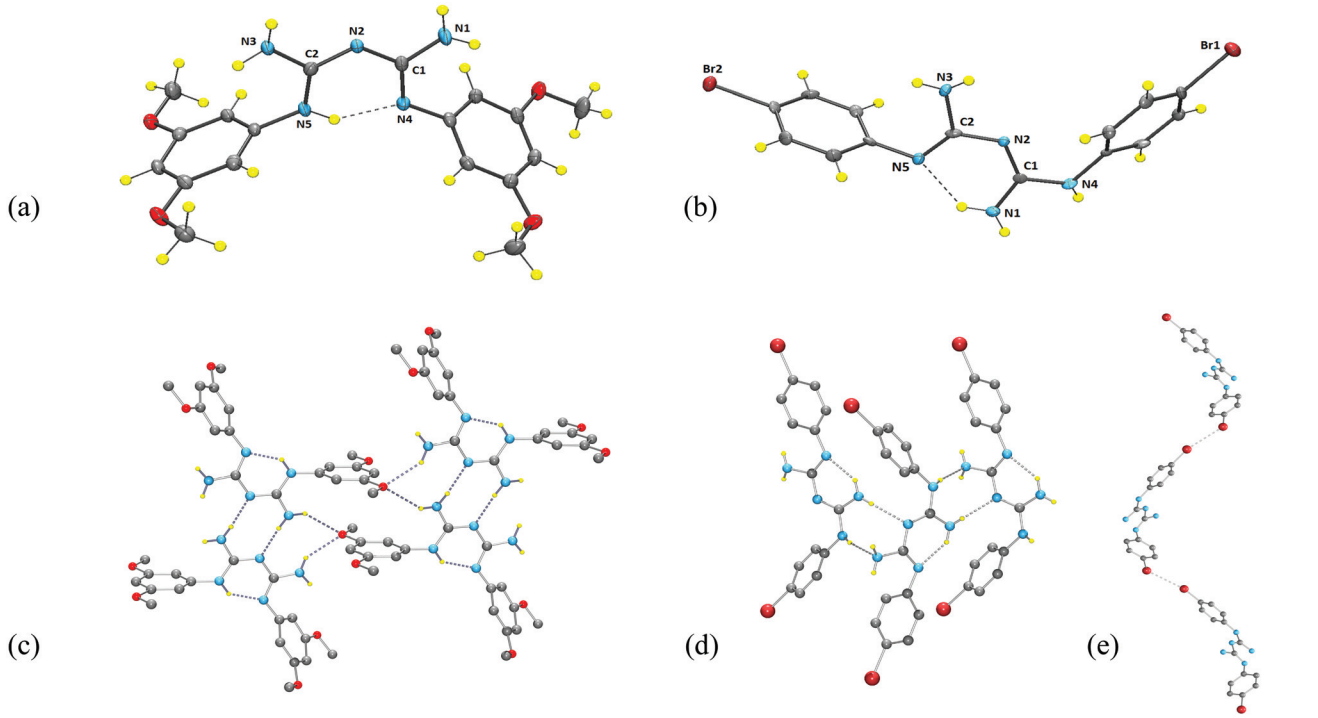

Fig. 3 X-ray structures of **HL3** (a) and **HL5** (b), with ellipsoids drawn at the 50% level. (c) Hydrogen bonding interactions joining adjacent **HL3** molecules. (d) Hydrogen bonding interactions, which assemble adjacent **HL5** molecules parallel to the *b* axis; (e) Br···Br interactions, which generate helical chains of **HL5** molecules parallel to the *c* axis. Non-NH hydrogens omitted for clarity.

The various phenyl substituents on **HL1–HL4** provide a subtle tuning of E_{pa} commensurate with their predicted inductive effect. Thus the 3,5-dimethylphenyl derivatives have nickel oxidation potentials *ca.* 30 mV lower than the phenyl derivatives, and the inductively negative 3,5-dimethoxyphenyl derivatives raise E_{pa} a similar amount.

X-Ray crystallography

The solid state structures of a number of the nickel(II) complexes, as well as two of the ligands were obtained by X-ray crystallography, in order to confirm the structures and explore the nature of the bonding within the chelate rings. Characterisation of the hydrogen bonding motifs present provides understanding of the potentials of these molecules for forming higher assemblies.

The structures of the ligands **HL3** and **HL5** are both found to exist in the expected tautomer (Scheme 1) with the central C2N5 unit being planar and stabilised by intramolecular hydrogen bonding. **HL3** crystallises in the triclinic space group $P\bar{1}$ with the asymmetric unit containing one ligand molecule (Fig. 3a, Table 2). An internal $R_1^1(6)$[29] hydrogen bond between N4 and the hydrogen atom on N5 stabilises the arrangement (Table 5). The OCH_3 groups are arranged in a *syn–anti* conformation on one of the aryl rings and in an *anti–anti* conformation on the other. Pairs of molecules are hydrogen bonded to each other by a $R_2^2(8)$ cyclic motif, involving N2 and a hydrogen atom on N3 in each molecule (Fig. 3c). These pairs are further hydrogen bonded into chains by $R_4^4(24)$ cyclic motifs, involving hydrogen atoms on the N3 atoms of two molecules and the O atoms in the OCH_3 groups in two molecules. The chains propagate parallel to the crystallographic *c* axis. The remaining aryl rings, not involved in this hydrogen bonding system, point out from the chain and interdigitate with related rings from the adjacent chains, stabilised by π–π stacking interactions (intercentroid distance is 3.840 Å, closest C···C distance 3.804 Å). In this way the chains are arranged into sheets lying parallel to the crystallographic *ab* diagonal.

The ligand **HL5** crystallises in the non-centric orthorhombic space group $P2_12_12_1$, with the asymmetric unit contains one ligand molecule (Fig. 3b, Table 2). The conformation

Table 2 Selected bond lengths (Å) and angles (°) for **HL3**, **HL5** and **HL1**[a]

	HL3	HL5	HL1
N1–C1	1.3580(18)	1.329(5)	1.321
C1–N2	1.3724(18)	1.322(5)	1.305
N2–C2	1.3408(17)	1.378(5)	1.378
C2–N3	1.3494(19)	1.395(5)	1.424
C1–N4	1.3168(18)	1.372(5)	1.388
C2–N5	1.3390(18)	1.298(5)	1.321
N1–C1–N2	113.06(13)	126.4(4)	126.73
N1–C1–N4	122.66(13)	115.4(4)	115.52
C1–N2–C2	121.25(12)	120.8(3)	120.75
N4–C1–N2	124.24(12)	118.1(3)	117.73
N2–C2–N3	116.57(13)	110.0(3)	110.59
N2–C2–N5	124.41(13)	126.9(4)	127.23
N3–C2–N5	118.98(13)	123.0(4)	121.87

[a] From ref. 5*a*.

of the **HL5** is very similar to that found for **HL1**,[5a] with an internal $R_1^1(6)$ hydrogen bond between N5 and one of the hydrogen atoms on N1 stabilising this arrangement (Table 5). Cyclic $R_2^2(8)$ hydrogen bonding motifs, involving NH and NH_2 protons on one molecule and the central N and an NH_2 (acting as an acceptor) on a second molecule, generate chains which run parallel to the crystallographic *b* axis (Fig. 3d, Table 5). Individual **HL5** molecules are also assembled into one-dimensional helical chains by Br···Br interactions (Br···Br distance is 3.59 Å), which run parallel to the crystallographic *c* axis and have a pitch of 26.8 Å (Fig. 3e). (The two aryl rings are at an angle of 82.76° to each other, giving the molecule a plane of chirality.) The combined effect of these two, orthogonal, intermolecular interactions is to generate chiral sheets of nested helical chains, all of which have the same handedness due to the non-centric space group.

X-ray structures of two of the cationic complexes were obtained, and in each, the anions were found to hydrogen bond to the complexes. In each case the pattern of CN bond lengths within the C2N5 core is the same as that previously reported[12] for coordinated neutral ligands with N_{donor}–C < N_{aryl}–C < N_{ring}–C and the C–N_{ring}–C angle being *ca.* 126° (Table 3). [Ni(**HL3**)]$(BF_4)_2(C_3H_6O)_2$ crystallises in the triclinic space group $P\bar{1}$. The asymmetric unit contains a Ni atom, positioned on a two-fold axis, one **HL3** ligand and a BF_4^- anion, along with an acetone solvate molecule (Fig. 4a, Table 3). The ligand adopts a *syn–syn* conformation, with the aryl rings lying almost parallel to each other. The OCH_3 groups on each of the rings are themselves in a *syn–anti* arrangement, with the groups on each ring arranged in the same way and lying in the plane of the aryl rings (Fig. 4a). The *syn–syn* conformation of the ligands means that the N_{ring}–H hydrogens are not available for hydrogen bonding. However, both the N_{donor}–H hydrogens and the N_{aryl}–H hydrogens are involved in relatively weak hydrogen bonds to the BF_4^- counterions (Table 5). Two of the fluorine atoms in the BF_4^- forming contiguous $R_2^1(6)$ hydrogen bonds to two N_{donor}–H hydrogens and to one N_{donor}–H and one N_{aryl}–H hydrogen, respectively (Table 5). The acetone oxygen hydrogen bonds to the remaining N_{aryl}–H hydrogen and then is further hydrogen bonded (more weakly) to the related N_{aryl}–H hydrogen on an adjacent $[Ni(\mathbf{HL3})_2]^{2+}$ cation. This, along with relatively strong π–π stacking interactions between aryl rings on adjacent cations (closest C···C distance is 3.48 Å) links the cations into chains that run parallel to the crystallographic *b* axis.

A small number of crystals of $[Ni(\mathbf{HL2})_2](ClO_4)_2(CH_3CN)_2$ were obtained after reaction of **HL2** with $Ni(ClO_4)_2$ rather than $Ni(BF_4)_2$. The complex crystallised in the triclinic space group

Table 3 Selected bond lengths (Å) and angles (°) for [Ni(**HL3**)$_2$]$(BF_4)_2$·C_3H_6O and [Ni(**HL2**)$_2$]$(ClO_4)_2$·$(CH_3CN)_2$

	[Ni(**HL3**)$_2$]$(BF_4)_2$·$(C_3H_6O)_2$	[Ni(**HL2**)$_2$]$(ClO_4)_2$·$(CH_3CN)_2$
Ni1–N1	1.854(4)	1.8582(16)
Ni1–N3	1.859(3)	1.8612(16)
N1–C1	1.286(5)	1.295(2)
C1–N2	1.362(5)	1.368(2)
N2–C2	1.363(5)	1.371(2)
C2–N3	1.294(5)	1.295(2)
C1–N4	1.356(5)	1.350(2)
C2–N5	1.360(5)	1.349(3)
N1–Ni1–N3	90.16(16)	89.66(7)
Ni1–N1–C1	130.8(3)	129.45(13)
N1–C1–N2	120.7(4)	121.06(16)
N1–C1–N4	123.0(4)	125.24(17)
C1–N2–C2	126.5(4)	125.27(16)
N4–C1–N2	116.2(3)	113.69(16)
N2–C2–N3	121.3(4)	120.83(17)
N2–C2–N5	115.5(4)	113.96(17)
C2–N3–Ni1	129.9(3)	129.58(13)
N3–C2–N5	123.1(4)	125.19(17)

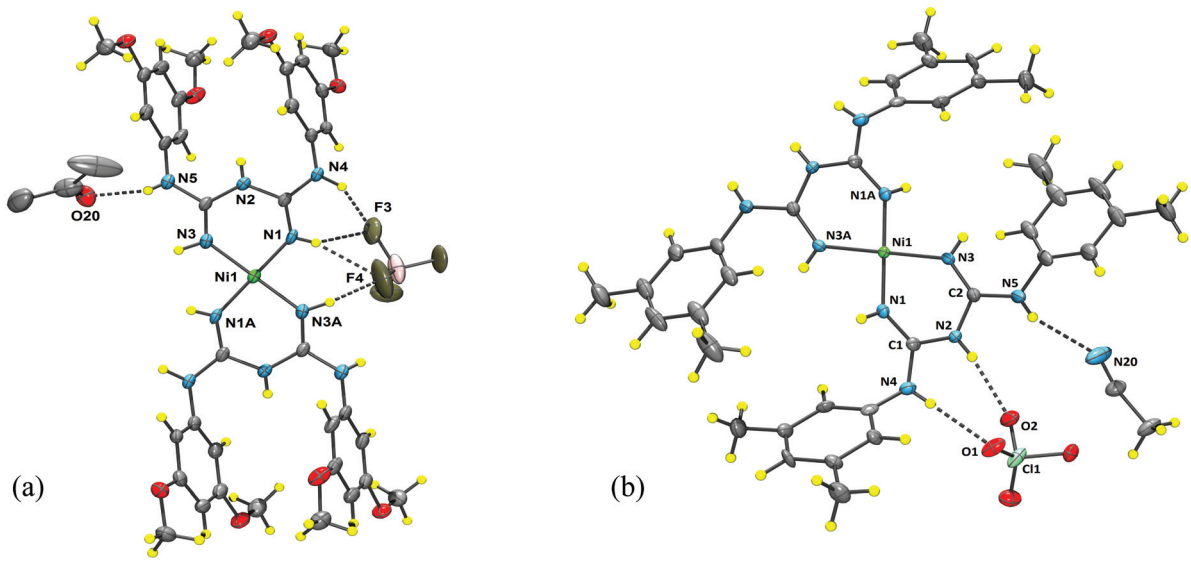

Fig. 4 X-ray structures of [Ni(**HL3**)$_2$]$(BF_4)_2$·C_3H_6O (a) and [Ni(**HL2**)$_2$]$(ClO_4)_2$·$(CH_3CN)_2$ (b), with ellipsoids drawn at the 50% level. Disordered aryl rings, perchlorate oxygens and acetonitrile carbons in [Ni(**HL2**)$_2$]$(ClO_4)_2$·$(CH_3CN)_2$ are omitted for clarity.

$P\bar{1}$ with the asymmetric unit containing a nickel(II) cation, lying on a two-fold rotation axis, one complete **HL2** ligand, one perchlorate anion and an acetonitrile solvate molecule (Fig. 4b, Table 3). Parts of the **HL2** ligand, the perchlorate anion and the acetonitrile molecule were disordered and were modelled appropriately (Experimental section). In contrast to the structure found for $[Ni(\mathbf{HL3})_2](BF_4)_2(C_3H_6O)_2$, the **HL2** ligands adopt an *anti–anti* conformation, meaning that the N_{donor}–H protons are not involved in hydrogen bonding interactions. Rather all three remaining NH groups act as donors, with adjacent N_{ring}–H and N_{aryl}–H groups hydrogen bonding to two oxygens of the perchlorate anion, forming a $R_2^2(8)$ motif. The third N_{aryl}–H hydrogen bonds to the nitrogen atom of the acetonitrile solvate molecule (Table 5).

The structures of two of the neutral complexes, containing deprotonated ligands, were also obtained. In the absence of anions, the complexes are found to hydrogen bond to solvent molecules and, in one case, to each other. In both cases the pattern of CN bond lengths within the C2N5 core is found to be the same as that previously reported for coordinated deprotonated ligands,[12] with N_{donor}–C < N_{ring}–C < N_{aryl}–C, and the C–N_{ring}–C angle is now decreased to *ca.* 120° (Table 4). $[Ni(\mathbf{L1})_2]$ is found to crystallise in the monoclinic space group *C*2/*c*, with the asymmetric unit containing a nickel(II) ion, lying on a two-fold rotation axis, two halves of a deprotonated **HL1** ligand and an acetonitrile solvate molecule (Fig. 5a, Table 4). The ligand adopts an *anti–anti* conformation, with aryl rings on different ligands within each $[Ni(\mathbf{L1})_2]$ arranged in a pseudo-orthogonal fashion. $[Ni(\mathbf{L1})_2]$ molecules are hydrogen bonded to each other by a $R_2^2(8)$ motif, involving the deprotonated N_{ring} nitrogen and one of the other N_{aryl}–H hydrogens (Fig. 5c). Adjacent molecules are not coplanar but rather lie with an angle of 45.49° between the NiN_4 planes, presumably due to the steric interactions between aryl rings. This cyclic hydrogen bonding motif joins adjacent molecules to generate chains which run along the crystallographic *ac* diagonal. The acetonitrile solvate molecules are hydrogen bonded *via* the nitrogen atom to the remaining N_{aryl}–H hydrogens, one per ligand (Table 5). The N_{donor}–H hydrogens are not involved in any hydrogen bonding interactions. The CH_3 group of each acetonitrile molecule lies above the nickel(II) ion of an adjacent $[Ni(\mathbf{L1})_2]$ hydrogen bonds between unit, forming a C–H···Ni anagostic interaction,[30] with an H···Ni distance of 2.83 Å and a C–H···Ni angle of 171.23°. The arrangement of the ligands is such that two acetonitrile molecules lie on the same side of the NiN_4 planes of adjacent $[Ni(\mathbf{L1})_2]$ units, bridging the nickel(II) ions and the NH donors. Thus adjacent $[Ni(\mathbf{L1})_2]$ units in the chain are assembled not only by the $R_2^2(8)$ cyclic hydrogen bonding but also by the hydrogen bonding/anagostic bonding of pairs of acetonitrile molecules (Fig. 5d).

$[Ni(\mathbf{L2})_2]\cdot(DMSO)_4$ crystallised in the triclinic space group $P\bar{1}$ with the asymmetric unit containing a nickel(II) ion, lying on a two-fold rotation axis, one deprotonated **HL2** ligand and two DMSO solvate molecules (Fig. 5b, Table 4). The ligand now adopts a *syn–anti* conformation. One of the DMSO molecules is hydrogen bonded to one of the N_{aryl}–H hydrogens while the other forms a bifurcated $R_2^2(6)$ hydrogen bond to the second N_{aryl}–H hydrogen and an adjacent N_{donor}–H hydrogen (Table 5). The remaining N_{donor}–H hydrogen is not involved in any hydrogen bonding interactions. Due to the presence of the DMSO molecules, there are no hydrogen bonding interactions between the $[Ni(\mathbf{L2})_2]$ units themselves.

Consideration of the packing of the molecules in the crystal shows that each of the DMSO molecules which are hydrogen bonded to the N_{aryl}–H hydrogen (only) form an $R_2^2(8)$ cyclic hydrogen bonding motif with a related DMSO molecule, which is, in turn, hydrogen bonded to an adjacent $[Ni(\mathbf{L2})_2]$ unit. In this way, chains of $[Ni(\mathbf{L2})_2]\cdot(DMSO)_4$ units are generated, which run parallel to the crystallographic *ab* diagonal (Fig. 5e).

In an initial set of experiments to ascertain the ways in which the deprotonated complexes might act as DAD hydrogen bonding motifs towards complementary organic molecules, each of the complexes were mixed with two equivalents of 1,8-naphthalimide in concentrated DMSO solutions. After standing at room temperature for some weeks, the solution containing $[Ni(\mathbf{L3})_2]$ gave some crystals suitable for X-ray analysis. The $[Ni(\mathbf{L3})_2]\cdot(1,8\text{-naphthalimide})_2$ assembly crystallised in the triclinic space group $P\bar{1}$, with the asymmetric unit containing half a nickel(II) ion, two halves of a deprotonated **L3** ligand and one molecule of 1,8-naphthalimide (Fig. 6, Table 4). The pattern of CN bond lengths within the C2N5 core is again the same as that previously reported for coordinated deprotonated ligands. The aryl arms of the **L3** ligand are in an *anti–anti* conformation, (as required for a DAD interaction) and the OCH_3 groups on each ring are in an *anti–anti* conformation with respect to their respective aryl rings.

The N_{aryl}–H hydrogens and the N_{ring} are involved in a DAD triple hydrogen bond with the 1,8-naphthalimide group, which is not coplanar to the NiN_4 plane, as found in related systems,[21,31] but rather is at an angle of 41.54°. The triple

Table 4 Selected bond lengths (Å) and angles (°) for $[Ni(\mathbf{L1})_2]\cdot(CH_3CN)_2$, $[Ni(\mathbf{L2})_2]\cdot(DMSO)_4$ and $[Ni(\mathbf{L3})_2]\cdot(1,8\text{-naphthalimide})_2$

	$[Ni(\mathbf{L1})_2]\cdot(CH_3CN)_2$	$[Ni(\mathbf{L2})_2]\cdot(DMSO)_4$	$[Ni(\mathbf{L3})_2]\cdot(1,8\text{ naphthalimide})_2$
Ni1–N1	1.851(2)	1.8539(11)	1.8497(17)
Ni1–N3	1.846(2)	1.8596(13)	1.8388(17)
N1–C1	1.315(3)	1.3290(15)	1.312(3)
C1–N2	1.338(3)	1.3389(15)	1.352(2)
N2–C2	1.346(3)	1.3501(15)	1.352(2)
C2–N3	1.319(3)	1.3201(15)	1.316(3)
C1–N4	1.380(3)	1.3854(15)	1.378(2)
C2–N5	1.363(3)	1.3774(15)	1.377(2)
N1–Ni1–N3	90.76(9)	89.36(5)	91.32(8)
Ni1–N1–C1	129.01(17)	129.00(8)	130.24(15)
N1–C1–N2	126.1(2)	126.60(11)	125.98(18)
N1–C1–N4	121.9(2)	116.21(10)	120.79(18)
C1–N2–C2	119.99(2)	119.15(10)	118.56(16)
N4–C1–N2	111.9(2)	117.17(10)	113.22(17)
N2–C2–N3	125.7(2)	126.76(10)	126.46(18)
N2–C2–N5	112.0(2)	111.88(10)	113.14(17)
C2–N3–Ni1	128.79(17)	128.88(9)	129.97(14)
N3–C2–N5	122.3(2)	121.35(11)	120.40(18)

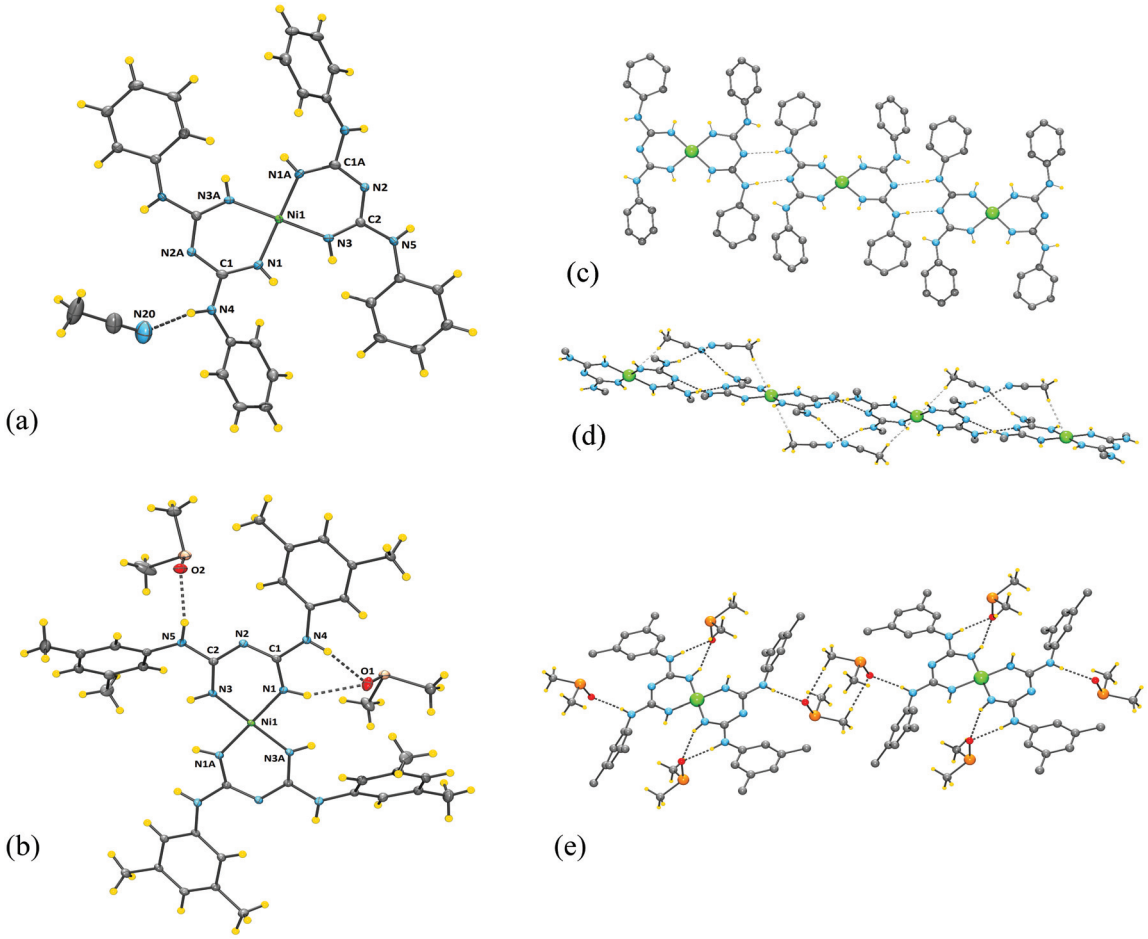

Fig. 5 X-ray structures of $[Ni(\mathbf{L1})_2]\cdot(CH_3CN)_2$ (a) and $[Ni(\mathbf{L2})_2]\cdot(DMSO)_4$, (b) with ellipsoids drawn at the 50% level. (c) Hydrogen bonding interactions joining adjacent $[Ni(\mathbf{L1})_2]$ molecules. Non-NH hydrogens and acetonitrile molecules omitted for clarity. (d) Hydrogen bonding and anagostic interactions joining adjacent $[Ni(\mathbf{L1})_2]$ molecules together *via* acetonitrile molecules. Aryl rings omitted for clarity. (e) Hydrogen bonding interactions joining adjacent $[Ni(\mathbf{L2})_2]\cdot(DMSO)_4$ molecules. Non-NH hydrogens omitted for clarity.

hydrogen bonding system can be described as a contiguous pair of $R_2^2(8)$ cyclic motifs. Adjacent $[Ni(\mathbf{L3})_2]\cdot$(1,8-naphthalimide)$_2$ units are held together by strong π–π stacking interactions between 1,8-naphthalimide units, which are parallel to each other (by symmetry) and 3.37 Å apart. These assemble the molecules into chains that run parallel to the crystallographic *b* axis (Fig. 6b, c). It is noted that a ^{1}H NMR titration experiment between $[Ni(\mathbf{L3})_2]$ and 1,8-naphthalimide was carried out in d_7-DMF and no evidence for association in this solution was observed, perhaps due to their being outcompeted by the solvent molecules.

Calculations

To provide further insight into the electronic and thermodynamic properties of the complexes, DFT calculations have been carried out. N–C bond lengths in the calculated structures of the complexes are listed in Table 6. These data clearly show that the characteristic patterns of bond lengths found in the X-ray crystals structures for the current $[Ni(\mathbf{HL})_2]^{2+}$ and $[Ni(\mathbf{L})_2]$ complexes, and in others in the literature,[12] are successfully reproduced by the calculations. Given that not all of the compounds have been crystallographically characterised, comparison of experimental and calculated vibration spectra provides a secondary way of validating calculations. Calculated FT Raman and IR spectra were compared to collected experimental spectra and were found to have a good correlation, with Mean Average Deviations (MAD) of 7–13 cm^{-1} (Fig. 7, S2–S9, Table S1†). Calculated, bond order changes with protonation/deprotonation are supported by observed band shifts in experimental FT-Raman and IR spectra for each pair of compounds. For $[Ni(\mathbf{L2})_2]$ and $[Ni(\mathbf{HL2})_2]^{2+}$, selected vibrational modes are shown in Fig. 8 and vibrational frequencies listed in Table 7.

Mode 129 of $[Ni(\mathbf{HL2})_2]^{2+}$ and mode 133 of $[Ni(\mathbf{L2})_2]$ are the same type of vibration, but the frequency of the vibration is shifted due to the change in bond order around the chelating nitrogens, as these bonds are involved in this vibration. In the FT-Raman spectrum of $[Ni(\mathbf{HL2})_2]^{2+}$, the band attributed to mode 129 is observed at 1014 cm^{-1}, while in the FT-Raman spectrum of $[Ni(\mathbf{L2})_2]$, the band attributed to this vibration (mode 133) is observed at 1036 cm^{-1}. Similarly in the IR spectra, the bands due to modes 209 and 222 of $[Ni(\mathbf{HL2})_2]^{2+}$

Table 5 Hydrogen bond lengths (Å) and angles (°)[a]

	d(D···A)	∠(D–H···A)
HL3		
N(5)–H(5)···N(4)	2.5940(17)	137.0(19)
N(1)–H(1A)···O(4)$^{\#1}$	3.0438(18)	144.9(14)
N(1)–H(1B)···O(4)$^{\#2}$	3.2441(17)	143.4(14)
N(3)–H(3A)···N(2)$^{\#3}$	2.9501(19)	175.0(17)
N(3)–H(3B)···O(4)$^{\#4}$	3.1944(16)	146.1(14)
HL5		
N1–H1A···N5	2.674(5)	129(4)
N1–H1B···N2$^{\#5}$	3.000(5)	176(4)
N4–H4B···N3$^{\#5}$	3.027(5)	170(5)
[Ni(**HL3**)$_2$](BF$_4$)$_2$·(C$_3$H$_6$O)$_2$		
N1–H1···F3	3.116(5)	140(3)
N1–H1···F4	3.298(8)	163(4)
N4–H4···F3	2.893(5)	149(4)
N3A–H3A···F4$^{\#6}$	2.957(5)	160(4)
N5–H5···O20	2.714(7)	162(5)
[Ni(**HL2**)$_2$](ClO$_4$)$_2$·(CH$_3$CN)$_2$		
N2–H2···O2	2.878(3)	171(2)
N4–H4···O1	2.806(4)	157(2)
N5–H5···N20	3.038(3)	129(2)
[Ni(**L1**)$_2$]·(CH$_3$CN)$_2$		
N4–H4···N20	3.219(3)	162(2)
N5–H5···N2$^{\#7}$	2.979(3)	174(2)
[Ni(**L2**)$_2$]·(DMSO)$_4$		
N1–H1···O1	3.0742(17)	154.4(15)
N4–H4···O1	2.8553(19)	164.0(15)
N5–H5···O2	2.9486(17)	158.7(14)
[Ni(**L3**)$_2$]·(1,8 naphthalimide)$_2$		
N4–H4···O6$^{\#8}$	2.868(2)	165(2)
N5–H5···O5	2.898(2)	158(2)
N6–H6B···N2	3.015(2)	168(2)

[a] Symmetry transformations: #1 $x, y, z-1$; #2 $-x, -y+1, -z$; #3 $-x+1, -y+2, -z$; #4 $-x+1, -y+2, -z+1$; #5 $-x+1, y-1/2, -z+1/2$; #6 $-x, -y, -z+1$; #7 $-x+2, y, -z+3/2$; #8 $-x+1, -y+1, -z$.

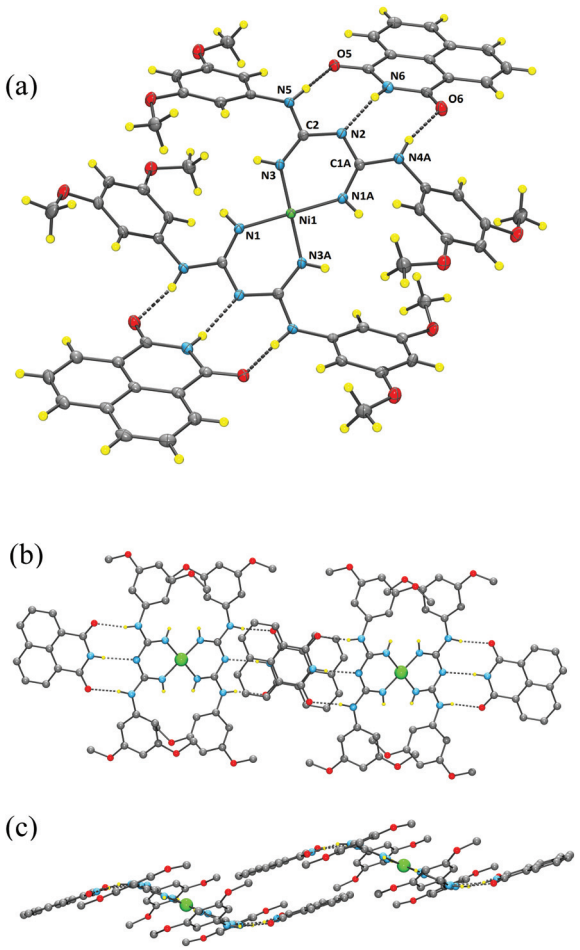

Fig. 6 (a) X-ray structure of [Ni(**L3**)$_2$]·(1,8-naphthalimide)$_2$, with ellipsoids drawn at the 50% level. Views down the *a* axis (b) and the *c* axis (c) of [Ni(**L3**)$_2$]·(1,8-naphthalimide)$_2$, showing the stacking interactions between 1,8-naphthalimide units. Non-NH hydrogens omitted for clarity.

are observed at 1508 and 1619 cm^{-1} respectively, and these correspond to modes 212 and 226 of [Ni(**L2**)$_2$] which are observed at 1564 and 1677 cm^{-1}, respectively (Fig. 7). Vibrational modes which significantly involve bonds which change order with protonation are expected to show a greater change in frequency.

TD-DFT calculations allow the visualisation of the molecular orbitals for the complexes (Fig. S11–S12†). In each case the HOMOs for the cationic complexes appear more diffuse than for the neutral complexes, with appreciable wavefunction amplitude across the aryl rings as well as the C2N3M rings, whereas the neutral systems show HOMOs which are confined to the C2N3M rings (Fig. 9). The calculations therefore confirm that, upon deprotonation, delocalisation of charge through the chelate ring to the metal ion occurs.

TD-DFT calculations also allow assignment of important transitions in the electronic spectra of the complexes. In DMF solution the cationic complexes were found to have a single band at *ca.* 445 nm, whereas in the neutral complexes, a band at *ca.* 436 nm, with a lower energy shoulder at *ca.* 490 nm, was found (above). In each case, extinction coefficients in the range *ca.* 100–160 mol^{-1} L cm^{-1} were found. TD-DFT calculations generally offset the absolute wavelength of transitions, but predict the nature of the transitions reasonably well. Thus, for each of the complexes three major transitions are found (Table S3†). These all have lower energies than those observed experimentally and are all predicted to be weak (oscillator strength ~0.0001) but of similar strength, making it difficult to assign which transition exactly corresponds to each experimental transition. The fact that the experimental data are collected in DMF solution, where there is the possibility of the complexes hydrogen bonding to solvent molecules, may go some way to explain the discrepancies between the calculated and experimental values. Nonetheless, the main findings from analysing these data are that: (1) the configurations that contribute significantly to the transitions all contain some HOMO and LUMO character (Fig. 9, S11, S12†), with all transitions terminating on the LUMO (which is quite similar between compounds); (2) the donor orbital set also possesses contribution from lower energy occupied orbitals, such as H-9, H-8 from Ni(**HL1**)$_2$ – these orbitals are by and large metal-based; (3) the deprotonated systems show a greater LUMO delocalisation than the protonated counterpart; (4) one of the transitions for each of the neutral complexes are significantly blue-shifted with respect to the corresponding cationic complexes.

Table 6 Calculated bond lengths (experimental bond lengths in parentheses)[a]

Complex	N_{ring}–C (Å)	N_{donor}–C (Å)	N_{aryl}–C (Å)
$[Ni(\mathbf{HL1})_2](BF_4)_2$	1.38595	1.30361	1.35609
$[Ni(\mathbf{HL2})_2](BF_4)_2$	1.38572	1.30364	1.35695
	(1.370)[b]	(1.295)[b]	(1.350)[b]
$[Ni(\mathbf{HL3})_2](BF_4)_2$	1.39174	1.32608	1.36914
	(1.363)	(1.290)	(1.358)
$[Ni(\mathbf{HL4})_2](BF_4)_2$	1.38449	1.30459	1.35609
$[Ni(\mathbf{L1})_2]$	1.34095	1.32095	1.39181
	(1.342)	(1.317)	(1.372)
$[Ni(\mathbf{L2})_2]$	1.34187	1.32094	1.39144
	(1.345)	(1.325)	(1.381)
$[Ni(\mathbf{L3})_2]$	1.34425	1.31815	1.39856
	(1.352)	(1.316)	(1.378)
$[Ni(\mathbf{L4})_2]$	1.34210	1.32013	1.39277

[a] Experimental values are averages of the two bond lengths found in the X-ray structure. [b] Data from the X-ray structure of $[Ni(HL2)_2](ClO_4)_2$.

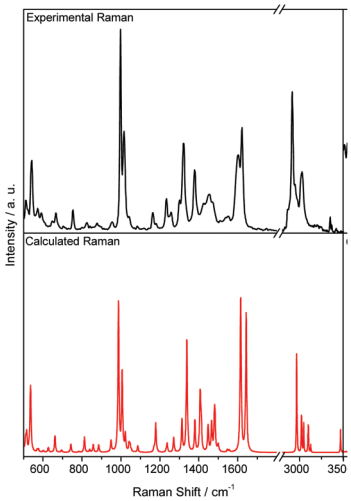

Fig. 7 Experimental and calculated Raman spectra for $[Ni(\mathbf{L2})_2]$.

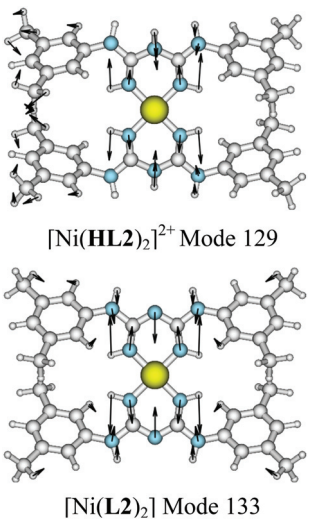

Fig. 8 Selected corresponding vibrational modes for $[Ni(\mathbf{L2})_2]$ and $[Ni(\mathbf{HL2})_2]^{2+}$.

Table 7 Comparison of experimental and calculated corresponding vibrational modes for $[Ni(\mathbf{HL2})_2]^{2+}$ and $[Ni(\mathbf{L2})_2]$, which display the consequences of the changes in bond order

Compound	Mode	Experimental frequency/cm^{-1}	Calculated frequency/cm^{-1}
$[Ni(\mathbf{HL2})_2]^{2+}$	129	1014	1006
$[Ni(\mathbf{HL2})_2]^{2+}$	209	1508	1514
$[Ni(\mathbf{HL2})_2]^{2+}$	222	1619	1633
$[Ni(\mathbf{L2})_2]$	133	1036	1020
$[Ni(\mathbf{L2})_2]$	212	1564	1547
$[Ni(\mathbf{L2})_2]$	226	1677	1670

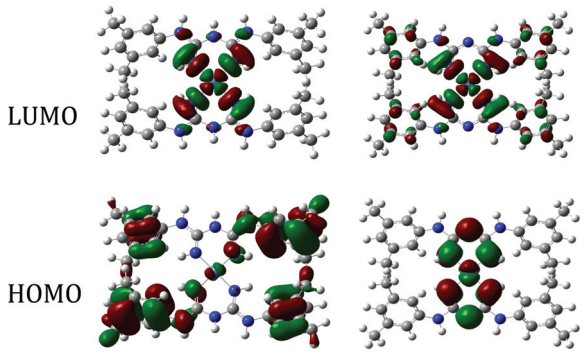

Fig. 9 Frontier molecular orbitals for $[Ni(\mathbf{HL2})_2](BF_4)_2$ (left) and $[Ni(\mathbf{L2})_2]$ (right). Note that the HOMO for $[Ni(\mathbf{HL2})_2](BF_4)_2$ is one of a pair of degenerate orbitals.

Conclusions

The work reported herein shows that 1,5-diarylbiguanides are readily prepared and effective ligands for nickel(II). Complexes containing either neutral or deprotonated biguanide ligands give complexes which can be characterised in solution and in the solid state. Various techniques show that, upon deprotonation, electron delocalisation within the chelate ring increases. Vibrational spectroscopy shows shifts in the band positions of the CN stretches, ^{1}H NMR spectroscopy shows shifts in the position of the peak corresponding to the N_{donor}–H hydrogens, and X-ray crystallography shows, upon deprotonation, a lengthening of the C–N_{donor} bonds and a lengthening of the C–N_{ring} bonds, along with a tightening of the C–N_{ring}–C bond angle, all of which are consistent with increased aromaticity in the chelate ring. UV-Visible spectroscopy shows small shifts of the absorption maximum upon deprotonation, consistent with the deprotonated ligands being better donors than the neutral ones and this is confirmed by cyclic voltammetry, which shows a stabilisation of the Ni(III) oxidation state upon deprotonation. X-ray crystal structures of the complexes allow the hydrogen bonding potential of these complexes to be assessed. The results presented here show that, while the electronic natures of the aryl ring substituents do play a subtle role in the electronic properties of the compounds, it is the conformation of the aryl rings themselves which is important in controlling the way in which the complex can hydrogen bond to other molecules. An *anti* orientation of the aryl ring with respect to the

central C2N5 core enables the associated N_{aryl}–H hydrogen to act as a donor, while the associated N_{donor}–H hydrogen becomes blocked by the aryl ring and unavailable for hydrogen bonding, whereas a *syn* orientation of the aryl ring blocks the N_{ring} hydrogen (or acceptor site in the deprotonated ligand) but enables hydrogen bonding of both the N_{aryl}–H and N_{donor}–H hydrogens. This work shows that these nickel(II) complexes have much potential as tectons for hydrogen-bonded assemblies, and that manipulation of the aryl ring substituents does offer promise for fine tuning the hydrogen bonding interactions. However, it is also clear that solvents such as DMF and DMSO readily compete for the NH donors, so current work is focused on assemblies with more soluble organic components and also other transition metal containing components with complementary hydrogen bonding motifs. In this way, it is hoped that assemblies with interesting chemical properties, as well as structural ones, might be realised.

Experimental section

Methods and materials

All reagents and metal salts were purchased commercially and used as received. ^{1}H NMR spectra were recorded on a 400 MHz Varian ^{UNITY}INOVA spectrometer at 298 K, referenced to the internal solvent signal. IR spectroscopy was carried out using a Bruker ALPHA FT-IR spectrometer with an ALPHA P ATR measurement module. ESI Mass Spectra were collected on a Bruker micro-TOF-Q spectrometer. UV/Visible spectra were recorded on a Perkin Elmer lambda 950 UV/VIS/NIR spectrometer. Microanalyses were performed at the Campbell Microanalytical Laboratory at the University of Otago. The ligands **HL1**–**HL5** were prepared following the general method described by Wuest.[5a] **HL1**, **HL2** and **HL5** have been reported previously.[5a] Cyclic voltammetric experiments in DMF were performed at 20 °C on solutions degassed with nitrogen. A three-electrode cell was used with Cypress Systems 1.4 mm diameter glassy carbon working, Ag/AgCl reference and platinum wire auxiliary electrodes. The solution was ~10^{-3} M in electroactive material and contained 0.1 M $[Bu_4N][PF_6]$ as the supporting electrolyte. Voltammograms were recorded with the aid of a Powerlab/4sp computer-controlled potentiostat. Potentials are referenced to the reversible formal potential (taken as E^o = 0.00 V) for the decamethylferricenium/decamethylferrocene ($[Fc^*]^{+/0}$) process,[32] where E^o was calculated from the average of the oxidation and reduction peak potentials under conditions of cyclic voltammetry. Under the same conditions, E^o calculated for $[FeCp_2]^{+/0}$ was 0.48 V *versus* $[Fc^*]^{+/0}$.[33] FT-Raman spectra were recorded on solid-state samples at room temperature using 184 scans per sample, at 4 cm^{-1} spectral resolution and 50 mW power. The excitation wavelength was 1064 nm, from a Nd:YAG laser source. A Bruker Equinox IFS-55 interferometer was used with a FRA/106 S attachment, and was controlled using the Bruker Opus v5.5 software package. Scattered Raman photons were detected using a liquid nitrogen cooled Ge diode (D418T). Spectral data was analysed using GRAMS/AI 8.00 (Thermo Electron Corporation) and OriginPro 8.0 (Origin Lab Corporation). Calculations were performed using the Gaussian09 package[34] and spectra extracted from calculations using GaussSum v2.2.5.[35] Geometry optimisation and frequency calculations utilised density functional theory (DFT) with a B3LYP functional, where a LANL2DZ basis set was used for nickel, and 6-31g(d) was used for all other atoms. Single point energy calculations *in vacuo* used the same parameters, while single point energy calculations in water required the inclusion of a solvent field, using the keyword "SCRF = (CPCM, solvent = water)". Calculated Raman and IR frequencies were scaled by 0.975, as DFT methods typically slightly overestimate the energy of vibrations. Calculated Raman intensities were scaled by eqn (5).[36] The "goodness of fit" between a calculation and experiment is quantified by the mean absolute deviation (MAD) between bands in the calculated and experimental IR and Raman spectra.

Syntheses

HL3. 3,5-Dimethoxyaniline (1.45 g, 9.5 mmol) was dissolved in 1 M HCl(aq) (10 mL). Sodium dicyanamide (0.40 g, 4.5 mmol) was added and the solution stirred at 100 °C for 18 hours. The solution was then cooled to room temperature and the resulting pale purple precipitate filtered off, washed with water and dried, to give 1.3 g of crude **HL3**·HCl. This was then suspended in dry methanol (10 mL) and a solution of sodium methoxide (1.5 mL, 25 wt%) was added. After stirring at room temperature for 1 hour, water (5 mL) was added and the resulting off-white solid filtered off, washed with water and dried *in vacuo*. Yield 0.92 g (55%). Mp 176–178 °C. Found: C, 57.78; H, 6.06; N, 18.84. Calc. for $C_{18}H_{23}N_5O_4$: C, 57.90; H, 6.21; N, 18.75%. HRESI-MS (CH_3OH) *m*/*z* 374.1818 [**HL3** + H] (calc. for $C_{18}H_{24}N_5O_4$ 374.1823 [**HL3** + H]$^+$). ^{1}H NMR (300 MHz, $CDCl_3$) δ 6.29 (m, 4H, H2, H6), 6.25 (m, 2H, H4), 3.79 (s, 12H, CH_3). IR ν_{max}/cm^{-1} 3430w, 3347w, 3083w, 2994w, 2918w, 2835w, 1575m, 1538m, 1454m, 1419m, 1355m, 1313m, 1241m, 1203m, 1191m, 1150s, 1096m, 1061m, 1044m, 990m, 959m, 927m, 868m, 853m, 837m, 812m, 766m, 724m, 679m, 644m, 610m.

HL4. This was prepared as for **HL3**, using 4-*t*-butylaniline (1.50 g, 10 mmol) and sodium dicyanamide (0.424 g, 4.8 mmol). The product was isolated as an off-white solid. Yield 1.581 g (90%). Mp 171–173 °C. Found: C, 72.10; H, 8.22; N, 19.43. Calc. for $C_{22}H_{31}N_5$: C, 72.30; H, 8.55; N, 19.15%. HRESI-MS (CH_3OH) *m*/*z* 366.2633 [**HL4** + H]$^+$ (calc. for $C_{22}H_{31}N_5$ 366.2652 [**HL4** + H]$^+$). ^{1}H NMR (300 MHz, $CDCl_3$) δ 7.36 (d, *J* = 8.4 Hz, 4H, H2, H6), 7.05 (d, *J* = 8.4 Hz, 4H, H3, H5), 3.50 (s, 1H, NH), 1.32 (s, 18H, CH_3). IR ν_{max}/cm^{-1} 3506w, 3430w, 3403w, 2958m 1671m, 1598s, 1548s, 1497m, 1389s, 1362m, 1256s, 841m, 752m.

$[Ni(HL1)_2](BF_4)_2$. $Ni(BF_4)_2{\cdot}6H_2O$ (41 mg, 0.13 mmol) was dissolved in acetone (2 mL) and added to a solution **HL1** (100 mg, 0.27 mmol) in acetone (4 mL) to give a clear orange-red solution. The solution was stirred for 1 hour, then concentrated and diethyl ether was added. The resulting pale orange

precipitate was filtered off, washed with diethyl ether and dried *in vacuo*. Yield 93 mg (64%). Found: C, 45.74; H, 4.13; N, 19.12. Calc. for $C_{28}H_{30}N_{10}NiB_2F_8$: C, 45.51; H, 4.09; N, 18.95%. HRESI-MS (DMF/MeCN) *m*/*z* 563.1927 [Ni(**HL1**)(**L1**)]$^+$ (calc. for $C_{28}H_{29}N_{10}Ni$ 563.1925 [Ni(**HL1**)(**L1**)]$^+$). ^{1}H NMR (300 MHz, DMF-d$_7$) δ 9.70 (s, 2H, NH), 7.60 (s, 4H, NH), 7.39 (d, 8H, CH), 7.33 (t, 8H, CH), 7.16 (t, 4H, CH), 7.07 (s, 4H, NH). IR ν_{max}/cm^{-1} 3378w, 3348w, 3318w, 3168w, 1660s, 1593s, 1548s, 1494s, 1461m, 1297m, 1247s, 1122m, 992s, 758s, 693s. UV/Vis (DMF) 448 nm (108 mol^{-1} L cm^{-1}).

[Ni(HL2)$_2$](BF$_4$)$_2$. This was prepared by the method described for [Ni(**HL1**)$_2$]. Yield 33%. Found: C, 50.66; H, 5.55; N, 16.19. Calc. for $C_{36}H_{46}N_{10}NiB_2F_8$: C, 50.80; H, 5.45; N, 16.45%. HRESI-MS (DMF/MeCN) *m*/*z* 675.3223 [Ni(**HL2**)(**L2**)]$^+$ (calc. for $C_{36}H_{45}N_{10}Ni$ 675.3177 [Ni(**HL2**)(**L2**)]$^+$). ^{1}H NMR (300 MHz, DMF-d$_7$) δ 9.50 (s, 2H, NH), 7.52 (s, 4H, NH), 6.99 (s, 4H, CH), 6.89 (s, 8H, CH), 6.70 (s, 4H, NH), 2.18 (s, 24H, CH$_3$). IR ν_{max}/cm^{-1} 3349m, 3325m, 3009w, 2917w, 1672s, 1618m, 1601m, 1567s, 1467s, 1325m, 1240m, 1144m, 1036s, 991s, 686s. UV/Vis (DMF) 446 nm (110 mol^{-1} L cm^{-1}).

[Ni(HL3)$_2$](BF$_4$)$_2$. This was prepared by the method described for [Ni(**HL1**)$_2$]. Yield 52%. Found: C, 45.89; H, 5.24; N, 13.52. Calc. for $C_{36}H_{46}N_{10}O_8NiB_2F_8{\cdot}2C_3H_6O$ C, 46.06; H, 5.34; N, 12.78%. HRESI-MS (DMF/MeCN) *m*/*z* 803.2743 [Ni(**HL3**)(**L3**)]$^+$ (calc. for $C_{36}H_{45}N_{10}O_8Ni$ 803.2770 [Ni(**HL3**)(**L3**)]$^+$). ^{1}H NMR (300 MHz, DMF-d$_7$) δ 9.66 (s, 2H, NH), 7.62 (s, 4H, NH), 6.61 (s, 4H, CH), 6.51 (s, 8H, CH), 6.18 (s, 4H, NH), 3.69 (s, 24H, CH$_3$). IR ν_{max}/cm^{-1} 3330w, 2938w, 1666s, 1596s, 1562s, 1458s, 1207m, 1154s, 1049s, 926m, 835m, 720m, 686m. UV/Vis (DMF) 440 nm (116 mol^{-1} L cm^{-1}).

[Ni(HL4)$_2$](BF$_4$)$_2$. This was prepared by the method described for [Ni(**HL1**)$_2$]. Yield 42%. Found: C, 54.41; H, 6.58; N, 14.18. Calc. for $C_{44}H_{62}N_{10}NiB_2F_8$: C, 54.86; H, 6.49; N, 14.53%. HRESI-MS (DMF/MeCN) *m*/*z* 787.4396 [Ni(**HL4**)(**L4**)]$^+$ (calc. for $C_{44}H_{61}N_{10}Ni$ 787.4429 [Ni(**HL4**)(**L4**)]$^+$). ^{1}H NMR (300 MHz, DMF-d$_7$) δ 9.61 (s, 2H, NH), 7.54 (s, 4H, NH), 7.37 (d, 8H, *J* = 8.8 Hz, CH), 7.31 (d, 8H, *J* = 8.8 Hz, CH), 7.27 (s, 4H, NH), 1.27 (36H, CH$_3$). IR ν_{max}/cm^{-1} 3354m, 2959w, 1655s, 1600m, 1552s, 1511s, 1462m, 1298m, 1263m, 1115m, 1016s, 840m, 750m, 713m. UV/Vis (DMF) 449 nm (119 mol^{-1} L cm^{-1}).

[Ni(L1)$_2$]. Ni(BF$_4$)$_2$·6H$_2$O (67 mg, 0.19 mmol) dissolved in warm CH$_3$OH (1 mL) was added to **HL1** (100 mg, 0.39 mmol) dissolved in warm CH$_3$OH (5 mL) to give a clear, deep red solution. Triethylamine (55 μL, 0.39 mmol) was added *via* syringe and the solution stirred for *ca.* 1 hour, resulting in the formation of a deep orange precipitate. This was filtered off, washed with methanol and diethyl ether and dried *in vacuo*. Yield 106 mg (95%). Found: C, 56.34; H, 5.37; N, 22.94. Calc. for $C_{28}H_{28}N_{10}Ni{\cdot}2H_2O$: C, 56.12; H, 5.38; N, 23.36%. HRESI-MS (DMF/MeCN) *m*/*z* 563.1967 [Ni(**HL1**)(**L1**)]$^+$ (calc. for $C_{28}H_{29}N_{10}Ni$ 563.1925 [Ni(**HL1**)(**L1**)]$^+$). ^{1}H NMR (300 MHz, DMF-d$_7$) δ 8.17 (s, 4H, NH), 7.35 (d, 8H, *J* = 7.6 Hz, CH), 7.20 (t, 8H, *J* = 7.6 Hz, CH), 6.93 (t, 4H, *J* = 6.8 Hz, CH). IR ν_{max}/cm^{-1} 3404w, 3184w, 3036w, 2929w, 1583m, 1494s, 1449s, 1275m, 1207m, 745s, 698s, 658s. UV/Vis (DMF) 436 nm (169 mol^{-1} L cm^{-1}).

[Ni(L2)$_2$]. This was prepared by the method described for [Ni(**L1**)$_2$]. Yield 72%. Found: C, 64.04; H, 6.54; N, 20.71. Calc. for $C_{36}H_{44}N_{10}Ni$: C, 64.01; H, 6.57; N, 20.73%. HRESI-MS (DMF/MeCN) *m*/*z* 675.3131 [Ni(**HL2**)(**L2**)]$^+$ (calc. for $C_{36}H_{45}N_{10}Ni$ 675.3177 [Ni(**HL2**)(**L2**)]$^+$). ^{1}H NMR (300 MHz, DMF-d$_7$) δ 7.95 (s, 4H, NH), 6.96 (s, 8H, CH), 6.57 (s, 4H, CH), 2.15 (s, 24H, CH$_3$). IR ν_{max}/cm^{-1} 3417w, 3202w, 2914w, 1601m, 1507s, 1459s, 1279s, 1177s, 1083m, 826m, 679s 665s. UV/Vis (DMF) 437 nm (108 mol^{-1} L cm^{-1}).

[Ni(L3)$_2$]. This was prepared by the method described for [Ni(**L1**)$_2$]. Yield 80%. Found: C, 52.68; H, 5.59; N, 17.06. Calc. for $C_{36}H_{44}N_{10}O_8Ni{\cdot}H_2O$: C, 52.63; H, 5.64; N, 17.04%. HRESI-MS (DMF/MeCN) *m*/*z* 803.2788 [Ni(**HL3**)(**L3**)]$^+$ (calc. for $C_{36}H_{45}N_{10}NiO_8$ 803.2770 [Ni(**HL3**)(**L3**)]$^+$). ^{1}H NMR (300 MHz, DMF-d$_7$) δ 8.15 (s, 4H NH), 6.57 (s, 8H, CH), 6.10 (s, 4H, CH), 3.68 (s, 24H, CH$_3$). IR ν_{max}/cm^{-1} 3407w, 3342w, 3199w, 2930w, 2836w, 1592s, 1509s, 1449s, 1429s, 1285m, 1192s, 1152s, 1065m, 801m, 702m, 681m. UV/Vis (DMF) 435 nm (137 mol^{-1} L cm^{-1}).

[Ni(L4)$_2$]. This was prepared by the method described for [Ni(**L1**)$_2$]. Yield 45%. Found: C, 62.48; H, 7.79; N, 16.39. Calc. for $C_{44}H_{60}N_{10}Ni{\cdot}3H_2O$: C, 62.78; H, 7.90; N, 16.63%. HRESI-MS (DMF/MeCN) *m*/*z* 787.4361 [Ni(**HL4**)(**L4**)]$^+$ (calc. for $C_{44}H_{61}N_{10}Ni$ 787.4429 [Ni(**HL4**)(**L4**)]$^+$). ^{1}H NMR (300 MHz, DMF-d$_7$) δ 8.05 (s, 4H, NH), 7.29 (d, 8H, *J* = 8.0 Hz, CH), 7.21 (d, 8H, *J* = 8.0 Hz, CH), 1.28 (s, 36H, CH$_3$). IR ν_{max}/cm^{-1} 3605w, 3422w, 3311w, 3050m, 2950w, 2899w, 1612m, 1583m, 1543m, 1504s, 1461s, 1304m, 1269m, 1242m, 1195m, 1065w, 823m, 681m. UV/Vis (DMF) 437 nm (153 mol^{-1} L cm^{-1}).

X-ray crystallography

Crystals of **HL3** and **HL5** were obtained by slow evaporation of methanol/water solutions. Crystals of [Ni(**HL3**)$_2$](BF$_4$)$_2$·(C$_3$H$_6$O) were obtained by diffusion of diethyl ether into an acetone solution. Crystals of [Ni(**HL2**)$_2$](ClO$_4$)$_2$·(CH$_3$CN)$_2$ were obtained by diffusion of diethyl ether into an acetonitrile solution. One of the **HL2** aryl rings was disordered over two coplanar positions, while the perchlorate anion and the acetonitrile solvate were also disordered over two sites, respectively. Crystals of [Ni(**L1**)$_2$]·(CH$_3$CN)$_2$ were obtained from slow evaporation of an acetonitrile solution of [Ni(**HL1**)$_2$](BF$_4$)$_2$. Crystals of [Ni(**L2**)$_2$]·(DMSO)$_4$ were obtained from a dimethyl sulfoxide solution at room temperature. Crystals of [Ni(**L3**)$_2$]·(1,8-naphthalimide)$_2$ were obtained from a dimethyl sulfoxide solution of the two reactants at room temperature. The crystal data, data collection and refinement parameters are listed in Table 8. All measurements were made with a Bruker Kappa ApexII area detector using graphite monochromatised Mo Kα (λ = 0.71073 Å) radiation. Intensities were corrected for Lorentz and polarisation effects[37] and for absorption using SADABS.[38] The structures were solved by direct methods using SHELXS[39] or SIR97,[40] running within the WinGX package[41] and refined on F^2 using all data by full-matrix least-squares procedures with SHELXL-97.[42] All non-hydrogen atoms were refined with anisotropic displacement parameters. Hydrogen atoms on carbon atoms were included in calculated positions with isotropic displacement parameters. Hydrogen atoms on nitrogen atoms

Table 8 Details of X-ray crystallographic data collection

	HL3	**HL5**	$[Ni(\mathbf{HL3})_2](BF_4)_2\cdot(C_3H_6O)_2$	$[Ni(\mathbf{HL2})_2](ClO_4)_2\cdot(CH_3CN)_2$	$[Ni(\mathbf{L1})_2]\cdot CH_3CN$	$[Ni\mathbf{L2})_2\cdot(DMSO)_4$	$[Ni(\mathbf{L3})_2$ (1,8-naphthalimide)$_2$
Empirical formula	$C_{18}H_{23}N_5O_4$	$C_{14}H_{13}Br_2N_5$	$C_{39}H_{46}B_2F_8N_{10}NiO_9$	$C_{20}H_{26}ClN_6Ni_{0.5}O_4$	$C_{32}H_{34}N_{12}Ni$	$C_{44}H_{68}N_{10}Ni_4S_4$	$C_{60}H_{58}N_{12}NiO_{12}$
Formula weight	373.41	411.11	1031.19	479.27	645.42	988.03	1197.89
Crystal system	Triclinic	Orthorhombic	Triclinic	Triclinic	Monoclinic	Triclinic	Triclinic
Space group	$P\bar{1}$	$P2_12_12_1$	$P\bar{1}$	$P\bar{1}$	$C2/c$	$P\bar{1}$	$P\bar{1}$
a/Å	8.961(2)	6.351(5)	7.9360(9)	8.059(5)	17.985(6)	8.701(5)	7.3986(3)
b/Å	10.019(2)	8.876(5)	8.5760(10)	8.919(5)	10.573(4)	11.840(5)	14.5430(8)
c/Å	10.989(2)	26.832(5)	17.863(2)	16.632(5)	18.103(6)	13.424(5)	14.5749(12)
α/°	75.650(11)	90	93.507(4)	101.045(5)	90	92.325(5)	116.861(4)
β/°	75.016(11)	90	90.073(4)	101.543(5)	114.717(19)	104.102(5)	96.539(4)
γ/°	80.808(13)	90	111.697(4)	98.542(5)	90	110.911(5)	98.148(3)
V/Å^3	918.5(4)	1512.6(15)	1127.1	1127.7(10)	3127.1	1240.4(10)	1356.50(15)
D_c/Mg m^{-3}	1.350	1.805	1.519	1.411	1.371	1.323	1.466
Z	2	4	1	2	4	1	1
μ/mm^{-1}	0.098	5.360	0.529	0.613	0.664	0.610	0.437
F(000)	396	808	532	502	1352	526	626
Dimensions/mm	0.29 × 0.21 × 0.06	0.45 × 0.37 × 0.05	0.50 × 0.30 × 0.10	0.26 × 0.20 × 0.17	0.60 × 0.16 × 0.12	0.54 × 0.36 × 0.13	0.58 × 0.23 × 0.20
θ range/°	2.11 to 27.55	2.42 to 26.51	1.14 to 24.79	2.43 to 27.24	2.48 to 24.94	2.60 to 34.89	1.64 to 25.64
Index ranges	$-11 \le h \le 11$ $-13 \le k \le 13$ $-14 \le l \le 14$	$-7 \le h \le 7$ $-8 \le k \le 10$ $-32 \le l \le 33$	$-9 \le h \le 8$ $-10 \le k \le 9$ $-20 \le l \le 21$	$-9 \le h \le 10$ $-11 \le k \le 11$ $-21 \le l \le 21$	$-21 \le h \le 21$ $-12 \le k \le 12$ $-21 \le l \le 17$	$-13 \le h \le 13$ $-18 \le k \le 14$ $-19 \le l \le 21$	$-8 \le h \le 8$ $-17 \le k \le 17$ $-17 \le l \le 17$
Reflections collected	31 150	26 016	18 212	38 990	20 854	34 673	40 825
Reflections unique	4201	2639	3771	4999	2715	10 423	5095
R_{int}	0.0564	0.0675	0.0368	0.469	0.0686	0.0443	0.0528
Completion (%)	99.2	95.7	97.9	98.9	98.8	96.4	99.6
Data/restraints/parameters	4201/0/272	2639/0/205	3771/0/351	4999/0/390	2715/0/222	10 423/0/310	5095/0/405
Goodness of fit on F^2	1.061	1.029	1.064	1.070	1.049	1.055	1.037
R_1, wR_2 (all data)	0.0658, 0.1195	0.0414, 0.0635	0.0777, 0.1815	0.0456, 0.0980	0.0511, 0.0873	0.0548, 0.1109	0.0482, 0.0872
R_1, wR_2 ($I > 2\sigma(I)$)	0.0433, 0.1092	0.0303, 0.0610	0.0600, 0.1633	0.0367, 0.0929	0.0361, 0.0806	0.0409, 0.1037	0.0362, 0.0806
Largest diff. peak and hole/e Å^{-3}	0.266, −0.245	0.578, −0.495	1.298, −1.226	0.565, −0.406	0.361, −0.346	0.730, −0.636	0.354, −0.331
Flack parameter		0.005(11)					

were found from the difference map and refined appropriately. The functions minimised were $\Sigma w (F_o^2 - F_c^2)$, with $w = [\sigma^2(F_o^2) + aP^2]^{-1}$, where $P = [\max(F_o)^2 + 2F_c^2]/3$. Crystallographic metrics were analysed using Mercury[43] and figures were produced using ORTEP[44] and POV-Ray.[45]

Acknowledgements

Dr James Crowley and Assoc Prof. Allan Blackman are thanked for helpful discussions, referees are thanked for helpful comments and the University of Otago is thanked for financial support.

References

1 (*a*) D. Fujita, A. Takahashi, S. Sato and M. Fujita, *J. Am. Chem. Soc.*, 2011, **133**, 13317; (*b*) M. Wang, Y.-R. Zheng, T. R. Cook and P. J. Stang, *Inorg. Chem.*, 2011, **50**, 6107; (*c*) C. A. Otter, P. J. Patty, M. A. K. Williams, M. R. Waterland and S. G. Telfer, *Nanoscale*, 2011, **3**, 941; (*d*) K. J. Kilpin, M. L. Gower, S. G. Telfer, G. B. Jameson and J. D. Crowley, *Inorg. Chem.*, 2011, **50**, 1123; (*e*) M.-J. Lin, A. Jouaiti, P. Grosshans, N. Kyritsakas and M. W. Hosseini, *Chem. Commun.*, 2011, 7635; (*f*) M.-C. Dul, E. Pardo, R. Lescouezec, Y. Journaux, J. Ferrando-Soria, R. Ruiz-Garcia, J. Cano, M. Julve, F. Lloret, D. Cangussu, C. L. M. Pereira, H. O. Stumpf, J. Pasan and C. Ruiz-Perez, *Coord. Chem. Rev.*, 2010, **254**, 2281; (*g*) M. Albrecht, M. Fiege and O. Osetska, *Coord. Chem. Rev.*, 2008, **252**, 812; (*h*) P. J. Steel, *Chem. N.Z.*, 2003, **67**, 57; (*i*) M. Schutte, C. Stolle and D. G. Kurth, *Supramol. Chem.*, 2003, **15**, 549.

2 D. A. McMorran, *Inorg. Chem.*, 2008, **47**, 592.

3 (*a*) D. Pogozhev, S. A. Baudron and M. W. Hosseini, *CrystEngComm*, 2010, **12**, 2238; (*b*) S. G. Telfer and J. D. Wuest, *Cryst. Growth Des.*, 2009, **9**, 1923; (*c*) C. Carpanese, S. Ferlay, N. Kyritsakas, M. Henry and M. W. Hosseini, *Chem. Commun.*, 2009, 6786; (*d*) K. Adachi, Y. Sugiyama, K. Yoneda, K. Yamada, K. Nozaki, A. Fuyuhiro and S. Kawata, *Chem.–Eur. J.*, 2005, **11**, 6616; (*e*) D. Braga, L. Brammer and N. R. Champness, *CrystEngComm*, 2005, **7**, 1; (*f*) S. Kitagawa and K. Uemura, *Chem. Soc. Rev.*, 2005, **34**, 109; (*g*) A. D. Burrows, C.-W. Chan, M. M. Chowdhry, J. E. McGrady and D. M. P. Mingos, *Chem. Soc. Rev.*, 1995, **24**, 329.

4 E. Bamberger and W. Dieckmann, *Ber.*, 1892, **25**, 543.

5 (*a*) O. LeBel, T. Maris, H. Duval and J. D. Wuest, *Can. J. Chem.*, 2005, **83**, 615; (*b*) A. R. Katritzky, S. R. Tala and A. Singh, *ARKIVOC*, 2010, 76; (*c*) O. Lebel, T. Maris and J. D. Wuest, *Can. J. Chem.*, 2006, **84**, 1426.

6 (*a*) D. Sweeney, M. L. Raymer and T. D. Lockwood, *Biochem. Pharmacol.*, 2003, **66**, 663; (*b*) N. P. Jensen, A. L. Ager, R. A. Bliss, C. J. Canfield, B. M. Kotecka, K. H. Rieckmann, J. Terpinski and D. P. Jacobus, *J. Med. Chem.*, 2001, **44**, 3925.

7 H. Tsubouchi, K. Ohguro, K. Yasumura, H. Ishikawa and M. Kikuchi, *Bioorg. Med. Chem. Lett.*, 1997, **7**, 1721.

8 M. Pollack, *Cancer Prev. Res.*, 2010, **3**(9), 1060.

9 N. Thakkar, V. Pirrone, S. Passic, S. Keogan, W. Zhu, V. Kholodovych, W. Welsh, R. Rando, M. Labib, B. Wigdahl and F. Krebs, *Antimicrob. Agents Chemother.*, 2010, **11**, 1965.

10 (*a*) K. M. Huttunen, A. Mannila, K. Laine, E. Kemppainen, J. Leppanen, J. Vepsalainen, T. Jarvinen and J. Rautio, *J. Med. Chem.*, 2009, **52**, 4142; (*b*) C. J. Bailey and R. C. Turner, *N. Engl. J. Med.*, 1996, **334**, 574.

11 P. Rây, *Chem. Rev.*, 1961, **61**, 313.

12 R. K. Ray and G. B. Kauffman, *Metal and Non-metal Biguanide Complexes*, New Age International Publishers, New Delhi, 1999.

13 (*a*) M. Zhu, L. Lu, P. Yang and X. Jin, *Acta Crystallogr., Sect. E: Struct. Rep. Online*, 2002, **58**, m272; (*b*) M. Zhu, L. Lu, P. Yang and X. Jin, *Acta Crystallogr., Sect. E: Struct. Rep. Online*, 2002, **58**, m217; (*c*) F. Bentefrit, B. Viossat, A. Tomas, D. Nguyen-Huy and G. Morant, *Ann. Pharm. Fr.*, 2002, **60**, 93; (*d*) F. Bentefrit, G. Morgant, B. Viossat, S. Leonce, N. Guilbaud, A. Pierre, G. Atassi and D. Nguyen-Huy, *J. Inorg. Biochem.*, 1997, **68**, 53; (*e*) P. Lemione, M. Chiadmi, V. Bissery, A. Yomas and B. Viossat, *Acta Crystallogr., Sect. C: Cryst. Struct. Commun.*, 1996, **52**, 1430; (*f*) B. Viossat, *Acta Crystallogr., Sect. C: Cryst. Struct. Commun.*, 1995, **51**, 878; (*g*) B. Viossat, *Acta Crystallogr., Sect. C: Cryst. Struct. Commun.*, 1995, **51**, 213.

14 (*a*) F. Bentefrit, P. Lemione, D. Nguyen-Huy, G. Morgant and B. Viossat, *Acta Crystallogr., Sect. C: Cryst. Struct. Commun.*, 2003, **59**, m331; (*b*) F. Bentefrit, A. Tomas, G. Morgant, D. Nguyen-Huy, P. Lemione, B. Viossat and Z. Kristallogr, *New Cryst. Struct.*, 2002, **217**, 505; (*c*) P. Spacu, C. Gheorghiu and A. Nicolaescu, *Inorg. Chim. Acta*, 1968, **2**, 413.

15 (*a*) A. De, *Acta Crystallogr., Sect. C: Cryst. Struct. Commun.*, 1990, **46**, 1004; (*b*) A. De, *J. Crystallogr. Spectrosc. Res.*, 1990, **20**, 279; (*c*) D. L. Ward, C. N. Caughlan and G. D. Smith, *Acta Crystallogr., Sect. B: Struct. Crystallogr. Cryst. Chem.*, 1971, **27**, 1541; (*d*) B. L. Holian and R. E. Marsh, *Acta Crystallogr., Sect. B: Struct. Crystallogr. Cryst. Chem.*, 1970, **26**, 1049; (*e*) N. R. Kunchur and M. Matthew, *Chem. Commun.*, 1966, 86.

16 (*a*) H. Kitamura, T. Ozawa, K. Jitsukawa, H. Masuda and H. Einaga, *Mol. Cryst. Liq. Cryst. Sci. Technol. Sect. A*, 2000, **342**, 69; (*b*) H. Kitamura, T. Ozawa, K. Jitsukawa, H. Masuda and H. Einaga, *Chem. Lett.*, 1999, 1225; (*c*) H. Kitamura, T. Ozawa, K. Jitsukawa, H. Masuda and H. Einaga, *Mol. Cryst. Liq. Cryst. Sci. Technol. Sect. A*, 1996, **285**, 281.

17 E. E. Simanek, X. Li, I. S. Choi and G. M. Whitesides, in *Comprehensive Supramolecular Chemistry*, ed. J. L. Atwood, J. E. D. Davies, D. D. MacNichol, F. Vögtle and J.-M. Lehn, Pergamon Press, New York, 1996, ch. 17, vol. 9, pp. 595–621.

18 (*a*) S. R. Saha, A. Bagchi and A. Das, *J. Indian Chem. Soc.*, 1990, **67**, 234; (*b*) P. Spacu, C. Gheorghiu and

A. Nicolaescu, *Inorg. Chim. Acta*, 1968, **2**, 411; (*c*) S. N. Poddar, *Sci. Cult.*, 1963, **29**, 308.

19 (*a*) W. Levason and M. D. Spicer, *Coord. Chem. Rev.*, 1987, **76**, 45; (*b*) C. R. Saha, *J. Inorg. Nucl. Chem.*, 1976, **38**, 1635; (*c*) A. K. Banerjee and S. P. Ghosh, *J. Indian Chem. Soc.*, 1976, **53**, 719.

20 P. Hubberstey and U. Suksangpanya, *Struct. Bonding*, 2004, **111**, 33.

21 M. M. Bishop, L. F. Lindoy, B. W. Skelton and A. H. White, *J. Chem. Soc., Dalton Trans.*, 2002, 377.

22 (*a*) M. M. Bishop, L. F. Lindoy, M. MaPartlin, A. Parkin, O. T. Thorn-Seshold and P. Turner, *Polyhedron*, 2007, **26**, 415; (*b*) M. M. Bishop, S. J. Coles, L. F. Lindoy and A. Parkin, *Inorg. Chim. Acta*, 2006, **359**, 3565.

23 (*a*) J. Tsuji, *Transition Metal Reagents and Catalyst: Innovations in Organic Synthesis*, John Wiley & Sons, England, 2000; (*b*) L. Brandsma, S. F. Vasilevsky and H. D. Verkruijsse, *Application of Transition Metal Catalysts in Organic Synthesis*, Springer, Berlin, 1998.

24 Cobalt(III): (*a*) T. Taha, Y. Kushi and H. Yoneda, *Bull. Chem. Soc. Jpn.*, 1982, **55**, 1063; (*b*) M. R. Snow, *Acta Crystallogr., Sect. B: Struct. Crystallogr. Cryst. Chem.*, 1974, **30**, 1850; (*c*) L. Coghi, M. Lanfranchi, G. Pelizzi and P. Tarascono, *Transition Met. Chem.*, 1978, **3**, 69; Chromium(III): (*d*) G. R. Brubaker and L. E. Webb, *J. Am. Chem. Soc.*, 1969, **91**, 7199; (*e*) L. Coghi, M. Nardelli and G. Pelizzi, *Acta Crystallogr., Sect. B: Struct. Crystallogr. Cryst. Chem.*, 1976, **32**, 842; Manganese(IV): (*f*) G. Das, P. K. Bharadwaj, D. Ghosh, B. Chaudhuri and R. Banerjee, *Chem. Commun.*, 2001, 323; (*g*) L.-P. Lu, M.-L. Zhu and P. Yang, *Acta Crystallogr., Sect. C: Cryst. Struct. Commun.*, 2004, **60**, m18; (*h*) R. O. C. Hart, S. G. Bott, J. L. Atwood and S. R. Cooper, *J. Chem. Soc., Chem. Commun.*, 1992, 894; Nickel(II) (*i*) Y.-L. Su, L.-P. Lu and M.-L. Zhu, *Acta Crystallogr., Sect. E: Struct. Rep. Online*, 2005, **61**, m2531; (*j*) T. C. Creitz, R. Gsell and D. L. Wampler, *Chem. Commun.*, 1969, 1371.

25 (*a*) P. V. Babykutty, C. P. Prabhakaran, R. Anantaraman and C. G. R. Nair, *J. Inorg. Nucl. Chem.*, 1974, **36**, 3685; (*b*) R. H. Skabo and P. W. Smith, *Aust. J. Chem.*, 1969, **22**, 659.

26 A. B. P. Lever, *Inorganic Electronic Spectroscopy*. Elsevier, Amsterdam, The Netherlands, 2nd edn, 1984.

27 (*a*) C. P. Joshua, A. George and M. Alaudeen, *J. Ind. Chem. Soc.*, 2004, **81**, 357; (*b*) B. Dutta and D. Sen, *Ind. J. Chem., A*, 1980, **19A**, 669; (*c*) S. Sen Gupta and D. Banerjea, *J. Ind. Chem. Soc.*, 1976, **53**, 741; (*d*) D. Sen and C. Saha, *J. Chem. Soc., Dalton Trans.*, 1976, 776.

28 A. Adenier, M. M. Chehimi, I. Gallardo, J. Pinson and N. Vila, *Langmuir*, 2004, **20**, 8243.

29 M. C. Etter, *Acc. Chem. Res.*, 1990, **23**, 120. For cyclic hydrogen bonding motifs, the designator R indicates a ring, the number of donors (d) and acceptors (a) found in the motif are assigned as subscripts and superscripts, respectively, and the number of atoms in the motif is indicated in parentheses. Thus $R_1^1(6)$ indicates a six membered ring motif comprising one donor and one acceptor.

30 (*a*) M. Brookhart, M. L. Gree and G. Parkin, *Proc. Natl. Acad. Sci. U. S. A.*, 2007, **104**, 6908; (*b*) W. I. Sundquist, D. P. Bancroft and S. J. Lippard, *J. Am. Chem. Soc.*, 1990, **112**, 1590.

31 A. Houlton, D. M. P. Mingos and D. J. Williams, *Transition Met. Chem.*, 1994, **19**, 653.

32 I. Noviandri, K. N. Brown, D. S. Fleming, P. T. Gulyas, P. A. Lay, A. F. Masters and L. Phillips, *J. Phys. Chem. B*, 1999, **103**, 6713.

33 F. Barriere and W. E. Geiger, *J. Am. Chem. Soc.*, 2006, **128**, 3980.

34 M. J. Frisch, G. W. Trucks, H. B. Schlegel, G. E. Scuseria, M. A. Robb, J. R. Cheeseman, G. Scalmani, V. Barone, B. Mennucci, G. A. Petersson, H. Nakatsuji, M. Caricato, X. Li, H. P. Hratchian, A. F. Izmaylov, J. Bloino, G. Zheng, J. L. Sonnenberg, M. Hada, M. Ehara, K. Toyota, R. Fukuda, J. Hasegawa, M. Ishida, T. Nakajima, Y. Honda, O. Kitao, H. Nakai, T. Vreven, J. A. Montgomery Jr., J. E. Peralta, F. Ogliaro, M. Bearpark, J. J. Heyd, E. Brothers, K. N. Kudin, V. N. Staroverov, R. Kobayashi, J. Normand, K. Raghavachari, A. Rendell, J. C. Burant, S. S. Iyengar, J. Tomasi, M. Cossi, N. Rega, J. M. Millam, M. Klene, J. E. Knox, J. B. Cross, V. Bakken, C. Adamo, J. Jaramillo, R. Gomperts, R. E. Stratmann, O. Yazyev, A. J. Austin, R. Cammi, C. Pomelli, J. W. Ochterski, R. L. Martin, K. Morokuma, V. G. Zakrzewski, G. A. Voth, P. Salvador, J. J. Dannenberg, S. Dapprich, A. D. Daniels, O. Farkas, J. B. Foresman, J. V. Ortiz, J. Cioslowski and D. J. Fox, *GAUSSIAN 09 (Revision A.02)*, Gaussian, Inc., Wallingford, CT, 2009.

35 N. M. O'Boyle, A. L. Tenderholt and K. M. Langner, *J. Comput. Chem.*, 2008, **29**, 839.

36 R. Horvath and K. C. Gordon, *Coord. Chem. Rev.*, 2010, **254**, 2505.

37 (*a*) *SAINT V4, Area Detector Control and Integration Software*, Siemens Analytical X-ray Systems Inc., Madison, WI, 1996; (*b*) Z. Otwinowski and W. Minor, in *Methods in Enzymology: Macromolecular Crystallography Part A*, ed. C. R. Carter Jr. and R. M. Sweet, Academic Press, 1997, vol. 276, p. 307.

38 G. M. Sheldrick, *SADABS, Program for Absorption Correction*, University of Göttingen, Germany, 1996.

39 G. M. Sheldrick, *SHELXS and SHELXL*, Institüt für Anorganische Chemie der Universität, Göttingen, Germany, 1996.

40 A. Altomare, M. C. Burla, M. Camalli, G. L. Cascarano, C. Giacovazzo, A. Guagliardi, A. G. G. Moliterni, G. Polidori and R. Spagna, *J. Appl. Crystallogr.*, 1999, **32**, 115.

41 L. J. Farrugia, *J. Appl. Crystallogr.*, 1999, **32**, 837.

42 G. M. Sheldrick, *Acta Crystallogr., Sect. A: Fundam. Crystallogr.*, 2008, **A64**, 112.

43 Mercury: visualization and analysis of crystal structures; C. F. Macrae, P. R. Edgington, P. McCabe, E. Pidcock, G. P. Shields, R. Taylor, M. Towler and J. van de Streek, *J. Appl. Crystallogr.*, 2006, **39**, 453.

44 L. J. Farrugia, *J. Appl. Crystallogr.*, 1997, **30**, 565.

45 http://www.povray.org/

